Tectonophysics 721 (2017) 415–434

Contents lists available at ScienceDirect

Tectonophysics

journal homepage: www.elsevier.com/locate/tecto

# Late Paleozoic and Mesozoic evolution of the Lhasa Terrane in the Xainza area of southern Tibet

Suoya Fan[a,b,*], Lin Ding[a], Michael A. Murphy[b], Wei Yao[a], An Yin[c]

[a] Key Laboratory of Continental Collision and Plateau Uplift, Institute of Tibetan Plateau Research, Chinese Academy of Sciences, Beijing 100101, China
[b] Department of Earth and Atmospheric Sciences, University of Houston, Houston, TX 77204, USA
[c] Department of Earth, Planetary, and Space Sciences, University of California, Los Angeles, CA 90095-1567, USA

ARTICLE INFO

*Keywords:*
Lhasa terrane
Shortening
Foreland basin
Suture zone
Provenance
Geochronology

ABSTRACT

Models for the Mesozoic growth of the Tibetan plateau describe closure of the Bangong Ocean resulting in accretion of the Lhasa terrane to the Qiangtang terrane along the Bangong-Nuijiang suture zone (BNSZ). However, a more complex history is suggested by studies of ophiolitic melanges south of the BNSZ "within" the Lhasa terrane. One such mélange belt is the Shiquanhe-Namu Co mélange zone (SNMZ) that is coincident with the Geren Co-Namu Co thrust (GNT). To better understand the structure, age, and provenance of rocks exposed along the SNMZ we conducted geologic mapping, sandstone petrography, and U-Pb zircon geochronology of rocks straddling the SNMZ. The GNT is north-directed and places Paleozoic strata against the Yongzhu ophiolite and Cretaceous strata along strike. A gabbro in the Yongzhu ophiolite yielded a U-Pb zircon age of 153 Ma. Detrital zircon age data from Permian rocks in the hanging wall suggests that the Lhasa terrane has affinity with the Himalaya and Qiangtang, rather than northwest Australia. The Late Jurassic- Early Cretaceous Rila Formation overlies the ophiolite and shows signatures of syntectonic deposition. Detrital zircon ages from the Cretaceous Duoni Formation in the footwall of the GNT suggest that the provenance is mainly Early Cretaceous igneous rocks in the northern Lhasa terrane and Paleozoic strata in the hanging wall of the GNT. Our results support the interpretation that the SNMZ is a Late Jurassic-Early Cretaceous suture zone that resulted from closure of a small Jurassic ocean basin, thereby suggesting more Jurassic shortening than conventional models. The GNT developed along the SNMZ in the Early Cretaceous and facilitated exhumation of Paleozoic strata, which became a source for Cretaceous basins along the GNT. Early Cretaceous igneous rocks in northern Lhasa are interpreted to be a consequence of subduction of ocean lithosphere along the SNMZ and its later delamination.

## 1. Introduction

The Tibetan plateau has been a locus of subduction-accretion events throughout the Mesozoic resulting in substantial crustal growth of the southern margin of the Asian continent. The suture zones recording these events have played major roles in tectonic models describing the kinematics of subduction (Bird, 1978; Yin et al., 1999; Chemenda et al., 2000; Kapp et al., 2000, 2007a; Zhang R. et al., 2011b), history of crustal growth (Yin and Harrison, 2000; Tapponnier et al., 2001; Zhu et al., 2011b), and, patterns of magmatism (Allégre et al., 1984; Coulon et al., 1986, Kapp et al., 2007a). The youngest accretion event prior to the India-Asia collision was the addition of the Lhasa terrane and other along-strike equivalent land masses to the southern margin of Asia (Metcalfe, 2009). It is widely thought that the Lhasa terrane collided with the southern margin of Asia (Qiangtang terrane) in the late Jurassic-Early Cretaceous and resulted in closure of the Bangong Ocean and formation of the Bangong-Nujiang suture zone (BNSZ) (Girardeau et al., 1984; Dewey et al., 1988; Yin and Harrison, 2000). Although, most tectonic models for the accretion of the Lhasa terrane interpret the Lhasa terrane to extend from the BNSZ in the north to the Indus-Yalu suture to the south, the existence of a semi-discontinuous mélange belt extending across the length of the Lhasa terrane suggests the presence of a suture zone within the Lhasa terrane (BGMRXAR, 1993; Hsü et al., 1995; Pan et al., 2012). The mélange belt extends from Nam Co in the east to Shiquanhe in the west and is referred to here as the Shiquanhe-Nam Co suture zone (SNMZ). Although SNMZ was mapped and studied during early investigations of the Lhasa terrane, it was interpreted to be a remnant of a far-traveled thrust rooted into the BNSZ (Girardeau et al., 1984; Coward et al., 1988) based on geologic mapping of what is interpreted to be a dismembered thrust sheet between Dongqiao and

* Corresponding author at: Department of Earth and Atmospheric Sciences, University of Houston, Houston, TX 77204, USA.
*E-mail address:* sfan2@uh.edu (S. Fan).

http://dx.doi.org/10.1016/j.tecto.2017.10.022
Received 11 April 2017; Received in revised form 29 September 2017; Accepted 20 October 2017
Available online 21 October 2017

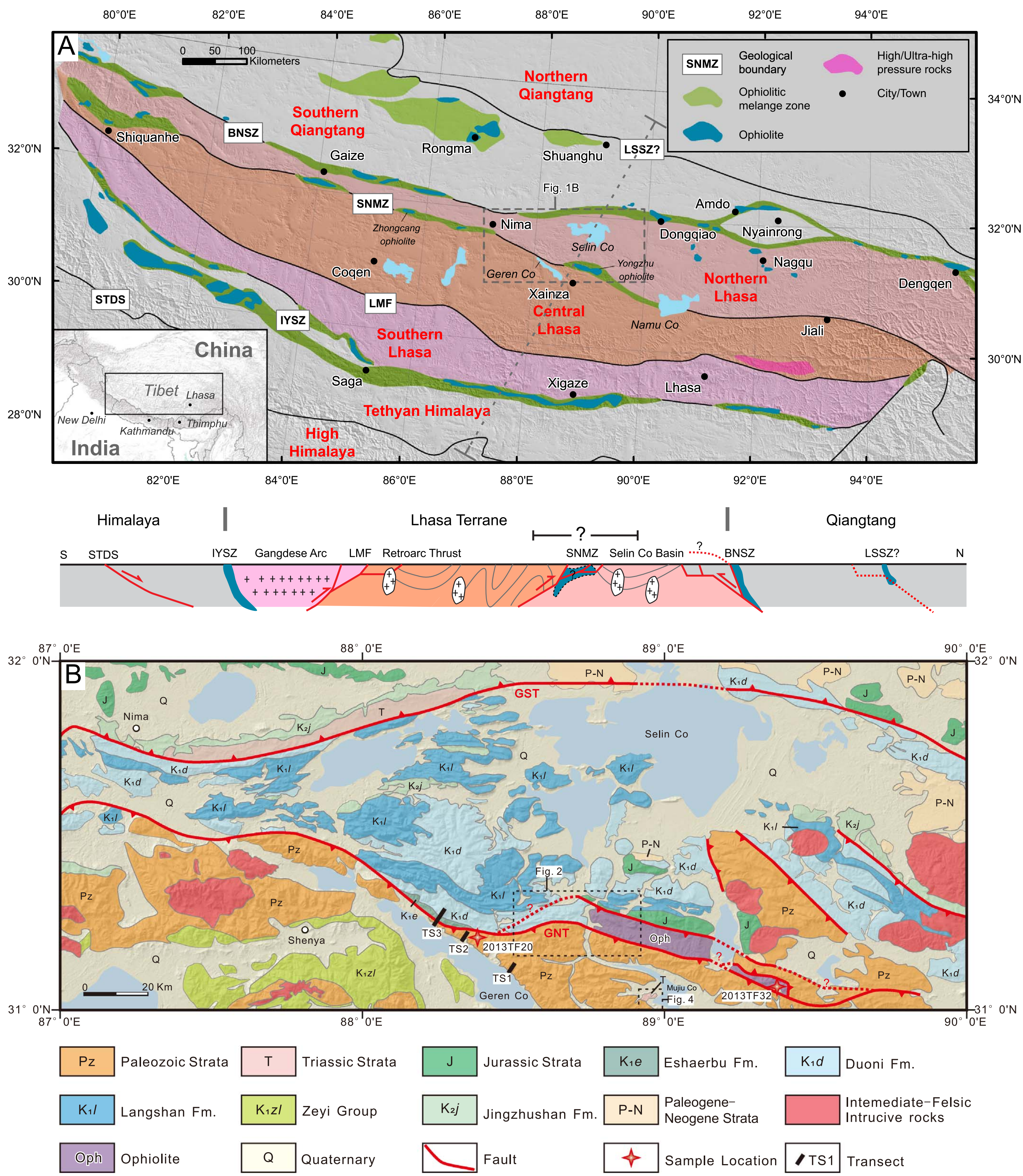


**Fig. 1.** (A) Tectonic framework of the Tibetan Plateau (adapted from Zhu et al., 2013) showing the location of the study area with respect to suture zones and fault systems. Abbreviations are LSSZ, Longmu Co-Shuanghu Suture Zone; BNSZ, Bangong-Nujiang Suture Zone; SNMZ, Shiquanhe-Nam Co Mélange Zone; LMF, Luobadui-Milashan Fault; IYSZ, Indus-Yarlung Suture Zone; STDS, South Tibetan Detachment System. (B) Simplified geologic map of the Selin Co area (modified from the 1:250,000 regional geological surveys in Tibet, Nima area and Duoba area). Abbreviations are GNT, Geren Co-Namu Co Thrust; GST, Gaize-Selin Co Thrust.

Geren Co (Fig. 1). However, further to the west the lack of evidence of a dismembered thrust sheet between the BNSZ and the SNMZ suggests that the SNMZ is a separate suture within the Lhasa terrane (Hsü et al., 1995), which is supported by major and trace element geochemistry studies (e.g. Wang et al., 2007; Xu et al., 2014; Ye et al., 2004; Zhong et al., 2015). Moreover, the geochronology of ophiolitic rocks from the BNSZ and the SNMZ are different. BNSZ rocks generally range from late Permian to Jurassic, while SNMZ rocks are younger (Jurassic to Early

Cretaceous, Tang et al., 2004; Zheng et al., 2006; Xu et al., 2014; Zhong et al., 2015; Zhang Y. X. et al., 2007a).

The SNMZ is defined by a laterally extensive thrust belt which we refer to as the Geren Co-Namu Co thrust (GNT) system. Locally, the GNT juxtaposes Paleozoic rocks in its hanging wall against Jurassic-Cretaceous strata in its footwall. Investigations of the provenance of Permian age strata have recently suggested that the Lhasa terrane was connected to the northwestern margin of Australia (e.g., Zhu et al., 2011a), and not to the Indian Gondwana system (Allégre et al., 1984; Yin and Harrison, 2000; Gehrels et al., 2011). Because the SNMZ is largely left out of tectonic models for the evolution of Tibetan crust data, from these rocks is scarce. In this contribution, we present a study of the structure, age, and provenance of rocks exposed along the central part of the SNMZ (88°E) (Fig. 1).

## 2. Geological setting

The Lhasa terrane is the southernmost Eurasian block speculated as having rifted from Gondwana and drifted northward across the Tethyan Ocean basins before it collided with Eurasia (Yin and Harrison, 2000; Zhu et al., 2011b). It is bounded by the Indus-Yarlung Zangbo suture zone (IYSZ) to the south and Bangong Nujiang suture zone (BNSZ) to the north (Allégre et al., 1984; Pan et al., 2004). Into 3 parts from north to south they are; Northern Lhasa, Central Lhasa, and Southern Lhasa (Pan et al., 2004, 2006; Zhu et al., 2011b) (Fig. 1A). The Northern Lhasa terrane is characterized by relatively juvenile crust with few crystalline basement rock exposures (Pan et al., 2004; Zhu et al., 2011b). Mesozoic and Cenozoic sequences widely outcrop there. The Lower Cretaceous sedimentary sequences contain abundant volcanic rocks, and contemporary plutonic bodies are also well documented (e.g. Pan et al., 2004; Zhu et al., 2009, 2011b; Qu et al., 2012). The Central Lhasa terrane contains Precambrian basement and the most complete Paleozoic sequence in the Lhasa terrane. It is interpreted to once be a microcontinent with Precambrian core (e.g. Pan et al., 2004; Zhu et al., 2011b, 2013). The Southern Lhasa terrane is characterized by a magmatic arc (Gangdese arc), which resulted from the northward subduction of the Neo-Tethyan ocean basin beneath the Lhasa terrane prior to the India-Asia collision (Yin and Harrison, 2000; Pan et al., 2004; Zhu et al., 2013; Zhang et al., 2012). Precambrian crystalline basement may locally exist as indicated by the emplacement of the early Paleozoic granite (Zhu et al., 2013).

The boundary between Northern Lhasa and Central Lhasa is the SNMZ (Fig. 1A) and coincides with a laterally extensive thrust belt referred to as the Geren Co-Namu Co thrust (GNT) system. Locally the thrust belt juxtaposes Paleozoic strata to the south against Jurassic-Cretaceous strata to the north. Ophiolitic rocks are exposed discontinuously along the SNMZ (BGMRXAR, 1993). The Yongzhu ophiolite is one of them. The age of this ophiolite is poorly documented. Attempts to estimate the age of the ophiolite using K-Ar, Rb-Sr, and individual zircon U-Pb dating methods bracket the age of the Yongzhu ophiolite to be from Jurassic to Cretaceous (e.g. Ye et al., 2004; Tang et al., 2004). Recently, a gabbro from the Zhongcang ophiolite in the SNMZ yielded zircon LA-ICP-MS U-Pb age of 114.3 ± 1.4 Ma (Xu et al., 2014). It remains a question whether these ophiolites were translated southwards in a thrust sheet rooted in the BNSZ (Girardeau et al., 1984, 1985; Coward et al., 1988; Kapp et al., 2003a) or represent an independent suture zone within the Lhasa terrane (Pan et al., 2006; Zhu et al., 2011b; Geng et al., 2011; Fu et al., 2015).

The boundary between Central Lhasa and Southern Lhasa is defined by the Luobadui-Milashan Fault (LMF) (Fig. 1A). It mainly juxtaposes Permian-Carboniferous strata in its hanging wall against a Jurassic-Cenozoic volcaniclastic sequence in its footwall (Pan et al., 2004; He et al., 2007). Recent studies of the high-pressure metamorphism, ultramafic rock geochemistry, SHRIMP U-Pb zircon geochronology, and $^{40}Ar/^{39}Ar$ muscovite thermochronology also suggest that the LMF might have formed within a Carboniferous-Permian suture zone and an orogenic event during Triassic (Chen et al., 2009; Li et al., 2003; Yang et al., 2009; Li et al., 2011). A 500–1000 m wide and at least 60 km long eclogite belt along it is documented. P-T calculations yielded peak metamorphic conditions of 2.7 GPa and 730 °C, and SHRIMP U-Pb dating of zircons from the eclogite yielded an average age of 262 ± 5 Ma (Yang et al., 2009) (Fig. 1A). $^{40}Ar/^{39}Ar$ dating of muscovite from a quartz schist and an amphibolite in the host rock yields ages between 200 and 240 Ma (Li et al., 2008, 2011). Single grain U-Pb zircon dating of a megaporphyritic granodiorite in the Gangdese batholith yields a crystallization age of 217.1 ± 3.4 Ma, which is interpreted to be associated with this orogenic event (Li et al., 2003).

The study area encompassing the town of Xainza straddles the central portion of SNMZ, covering both Northern Lhasa and Central Lhasa (Fig. 1A). The Yongzhu ophiolite and several thrust faults are exposed along the SNMZ in the middle of the study area (Fig. 1B). The most complete sequence of Paleozoic strata in the Lhasa terrane crops out to the south of the SNMZ. A key issue concerning the Paleozoic strata issue is the plate position and sedimentary affinity of the Lhasa terrane in the Late Paleozoic. It has long been thought that Lhasa terrane separated from the northern margin of the Indian plate (Allégre et al., 1984; Yin and Harrison, 2000; Metcalfe, 2009; Gehrels et al., 2011). However, Zhu et al. (2010, 2011a) challenged this idea based on the U-Pb age and Hf isotope data on detrital zircons from Paleozoic metasedimentary rocks in the Lhasa terrane and proposed that it separated from Australia and was an isolated microcontinent in Tethys Ocean in the Permian. However, Gehrels et al. (2011) still favors the previous view, even though both of their arguments invoked age data of zircons as important evidence. The differences in these conclusions may be due to the small numbers and distribution of samples analyzed.

Triassic strata are almost absent in the northern part of the Lhasa terrane except to the east of Mujiu Co in the Xainza area (Fig. 1B) which may explain why the evolution of northern part of the Lhasa terrane during the Triassic is poorly understood. Jurassic strata are abundant in Northern Lhasa subterrane, especially near the BNSZ. Cretaceous strata are exposed throughout the central part of the Northern Lhasa subterrane. The tectonic setting of these sedimentary basins and the associated faults remains poorly understood. Existing models include: (1) a backarc extensional basin in the northern Lhasa terrane (Zhang et al., 2012); (2) a retroarc foreland basin induced by the north-directed retroarc foreland thrusts to the north of Gangdese arc (Zhang Q. H. et al., 2011a; Leier et al., 2007a); (3) a peripheral foreland basin induced by the south-directed foreland thrusts rooted in the BNSZ, with some north-directed back thrusts or passive roof thrusts (Kapp et al., 2003a, 2007a; Volkmer et al., 2007, 2014; Murphy et al., 1997; DeCelles et al., 2007; Leier et al., 2007b).

## 3. Tectonostratigraphy of the Xainza area

### 3.1. Paleozoic strata

The Xainza area has the most complete exposure of Paleozoic strata in the Lhasa terrane, containing sedimentary rock sequences from Ordovician to Permian (Leeder et al., 1988; Yin et al., 1988; Pan et al., 2004). The base of what previously thought to be Ordovician might be Cambrian according to Gehrels et al. (2011). Among them, Devonian, Carboniferous, and Permian strata are the most commonly exposed (Fig. 2).

Early Paleozoic stratigraphic sequences mainly contain carbonate and shale, with lesser amounts of clastic rocks. Carboniferous strata are represented by the Yongzhu Formation ($C_{1-2}y$) that consists of sandstone, metasandstone, wacke, and shale. They are interpreted to be deposited in a marine environment, and locally contain glacial-marine diamictite, which are extensively exposed in the Tethyan Himalaya (Jin, 2002) and northern and western Australia (Eyles and Eyles, 2000; Eyles et al., 2006). The Lower Permian, Angjie Formation ($P_1a$) is mainly composed of sandstone, metasandstone, wacke, shale, and

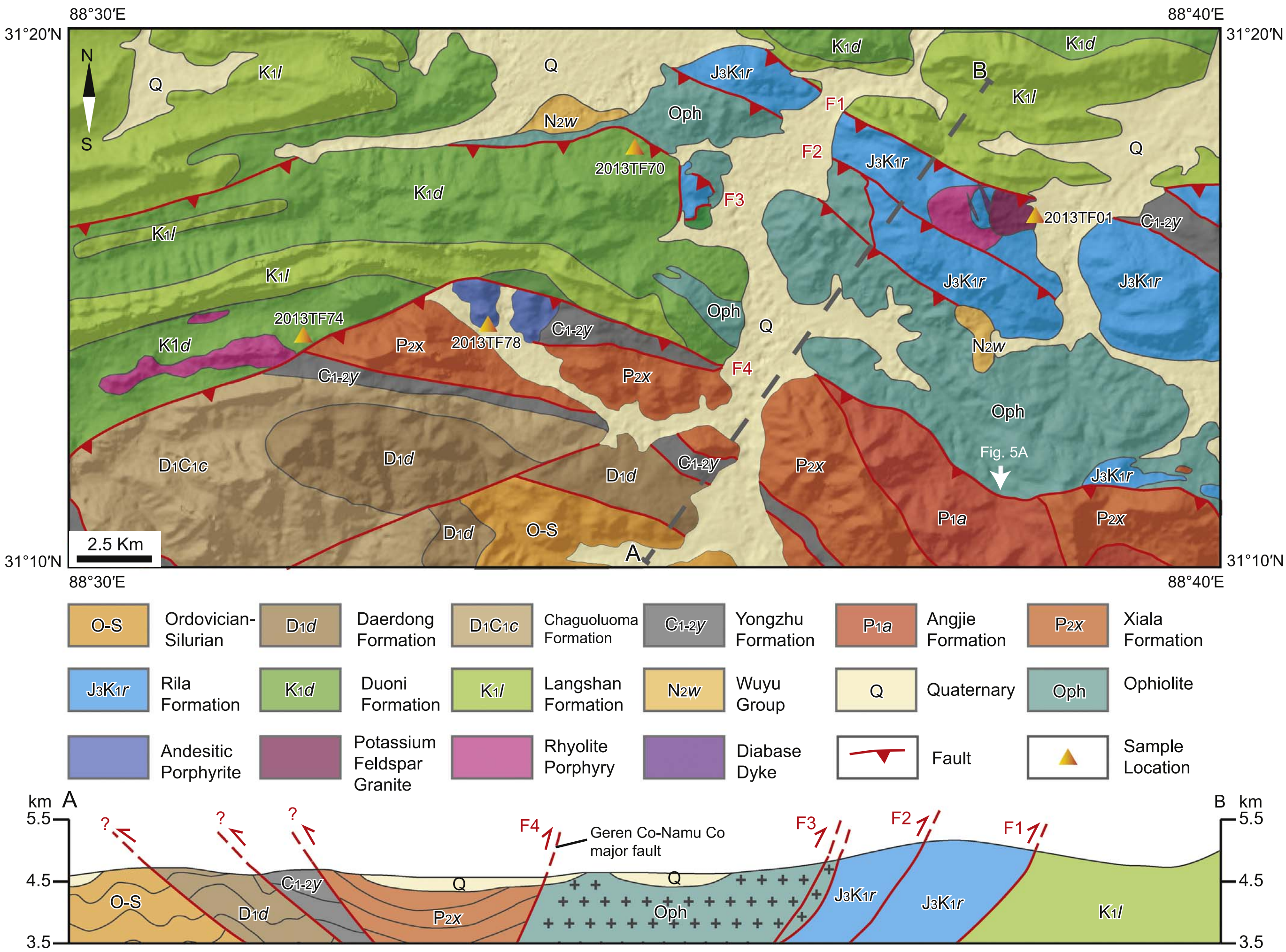


**Fig. 2.** Geologic map of the area north of Xainza city (modified from the 1:250,000 regional geological surveys in Tibet, Duoba area, and our own observations).

mudstone (Fig. 3). It partly contains flysch represented by a 200 m-thick sequence of interbedded sandstone and shale (Fig. 3A). The Angjie Formation, from the bottom to the top, is composed of yellow-brown wacke (Fig. 3B), medium-to-coarse-grained white sandstone (Fig. 3C), black bioclastic fossil-bearing limestone (Fig. 3D), thinly bedded shale (Fig. 3E), limestone containing chert pebbles (Fig. 3F), conglomerate (Fig. 3G), and siltstone (Fig. 3H). Their position in the stratigraphic section is shown in Fig. 3. Middle and upper Permian strata are represented by the Xiala Formation ($P_2x$) and Mujiucuo Formation ($P_3m$). Both primarily consist of limestone and dolomite.

### 3.2. Triassic strata

Outcrops of Triassic strata are rare in the north part of the Lhasa terrane. In the Xainza area, only some Upper Triassic, Duoburi Formation ($T_3d$), outcrops to the west of Mujiu Co (Fig. 4). It unconformably overlies the Late Permian Mujiuco Formation, and is intruded by a megaporphyritic granodiorite (Qu et al., 2003a). Their age is constrained by fossil assemblages in the limestone. The lower portion of Duoburi Formation mainly consists of sandstone, wacke, and mudstone, which are interbedded with limestone. Limestone is more common at the top of the formation.

### 3.3. Jurassic-Cretaceous strata

The Late Jurassic-Early Cretaceous Rila Formation ($J_3K_1r$) contains conglomerate, limestone, siltstone, and radiolarian chert. The age is constrained by a radiolarian fossil assemblage (Qu et al., 2003b). The Rila Formation overlies the Yongzhu ophiolite, therefore, placing a minimum age constraint on the closing of this marine basin of Late Jurassic-Early Cretaceous (Fig. 5). The basal limestone of the Rila Formation is strongly deformed. The upper part of the limestone is medium-thick bedded. (Fig. 5). Bedding in the chert is highly disturbed, and the chert locally contains large limestone blocks which could be olistostromes (Fig. 6A). Fault breccia is locally exposed along the fault F2 (Figs. 2, 6B).

The Cretaceous sequences from oldest to youngest are the Eshaerbu Formation ($K_1e$), Duoni Formation ($K_1d$) or Zeyi group ($K_1zl$), Langshan Formation ($K_1l$), and Jingzhushan Formation ($K_2j$) (Fig. 7). They are extensively exposed in Selin Co area. For a detailed description of the stratigraphy and sedimentology refer to Zhang et al. (2011a).

The Eshaerbu Formation is only exposed north of Geren Co. It mainly contains interbedded sandstone, laminated mudstone and siltstone interpreted to be deposited in a submarine fan and basin plain environment (Zhang Q. H. et al., 2011a). The lowest part of the sequence is interpreted as flysch facies displaying a complete Bouma sequence. The Duoni Formation crops out extensively in Selin Co and Lunpola areas, and consists of pebbly conglomerate, pebbly sandstone, and mudstone, which are interpreted as submarine fan and river delta deposits (Zhang Q. H. et al., 2011a; Leier et al., 2007b). It is common that Duoni Formation contain intermediate-felsic volcanic rocks. In some areas, like the Shenya area west of Geren Co, volcanic rocks dominate the Formation with relatively less clastic sedimentary rocks than the Duoni Formation. They are referred to as the Zeyi Group,

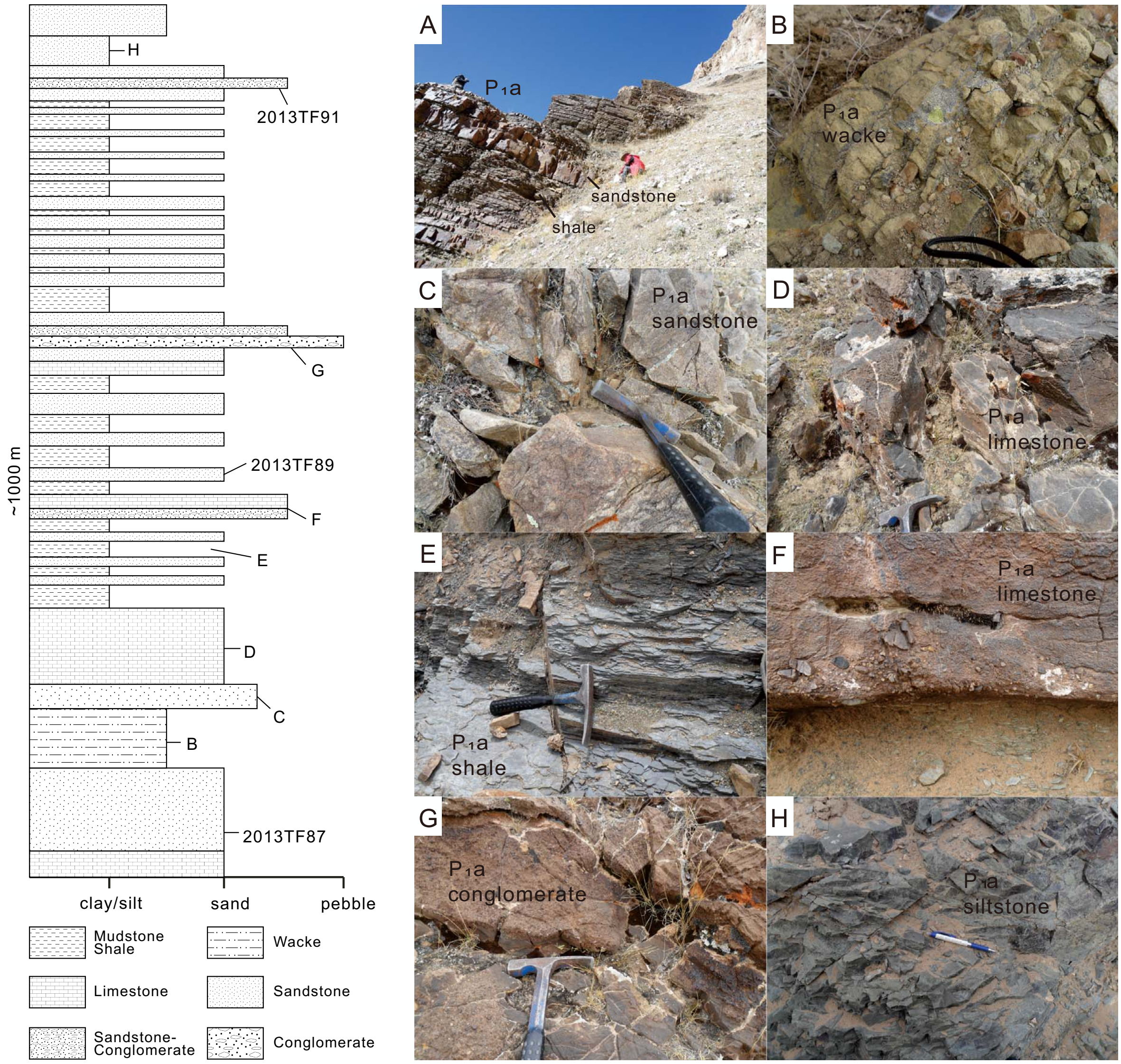


**Fig. 3.** Schematic stratigraphic column and photos of the Angjie Formation in Transect 2 (TS2 in Fig. 1B). 2013TF87, 2013TF89, 2013TF91 are samples collected from this transect. A is flysch-type sequence containing interbedded shale and sandstone. It is the location of sample 2013TF20 (refer to Fig. 1). B–H are different types of rocks exposed in TS2. Their positions in TS2 are shown in the stratigraphic column.

which chronostratigraphically correlates to the Duoni Formation and/or Langshan Formation. The Langshan Formation is well exposed in the Selin Co basin. It consists of dark-gray rudist and orbitolinoid-dominated mudstone, wackestone, and bioclastic packstone. It is interpreted to be deposited in a shallow marine carbonate platform environment (Pan et al., 2004; Zhang Q. H. et al., 2011a). The Jingzhushan Formation consists of red medium-to-coarse-grained sandstone and mottled pebble-cobble conglomerate which coarsens upward. The clast composition of the conglomerate suggests it was derived from limestones in the uplifted Langshan Formation in the Nima basin deposits (DeCelles et al., 2007). The depositional environment is interpreted to be a subaerial alluvial fan (Zhang Q. H. et al., 2011a).

### 3.4. Cenozoic strata

Cenozoic strata in Selin Co area include the: Niubao Formation ($E_{1-2}$n), Dingqinghu Formation ($E_3$d), and Wuyu Group ($N_2$w). They mainly consist of clastic rocks, including conglomerate, sandstone, and shale interbedded with minor volcanic beds. The conglomerates and sandstones of Wuyu Group are undeformed and unconformably overlie the Yongzhu ophiolite. The overlying Wuyu group consists of a basal conglomerate which grades upward to sandstone. Cobbles in the basal conglomerate are subrounded to subangular and range up to 5 cm in diameter, indicating a proximal source.

### 3.5. Yongzhu ophiolite

The Yongzhu ophiolite crops out along the middle segment of the Shiquanhe – Namu Co mélange zone (SNMZ), which is considered as the boundary between the Northern Lhasa subterrane and Central Lhasa subterrane. The east-west striking Yongzhu ophiolite zone is about 80 km long and as much as 9 km wide. It is separated from Paleozoic and Mesozoic strata by north-directed thrust faults and is unconformably overlain by the Wuyu group.

Outcrops of the ophiolite expose a variety of rock types including peridotite, pyroxene cumulates, sheeted dikes, pillow basalt, and radiolarian chert. Mafic sheeted dikes outcrop in the southeast part of the Yongzhu ophiolite belt. The dikes are mainly gabbro and diabase. The width of the dikes varies from 0.5–5 m (Fig. 6C). The peridotite and pillow basalt are intruded by mafic dikes and the peridotite is unconformably overlain by limestone of Rila Formation.

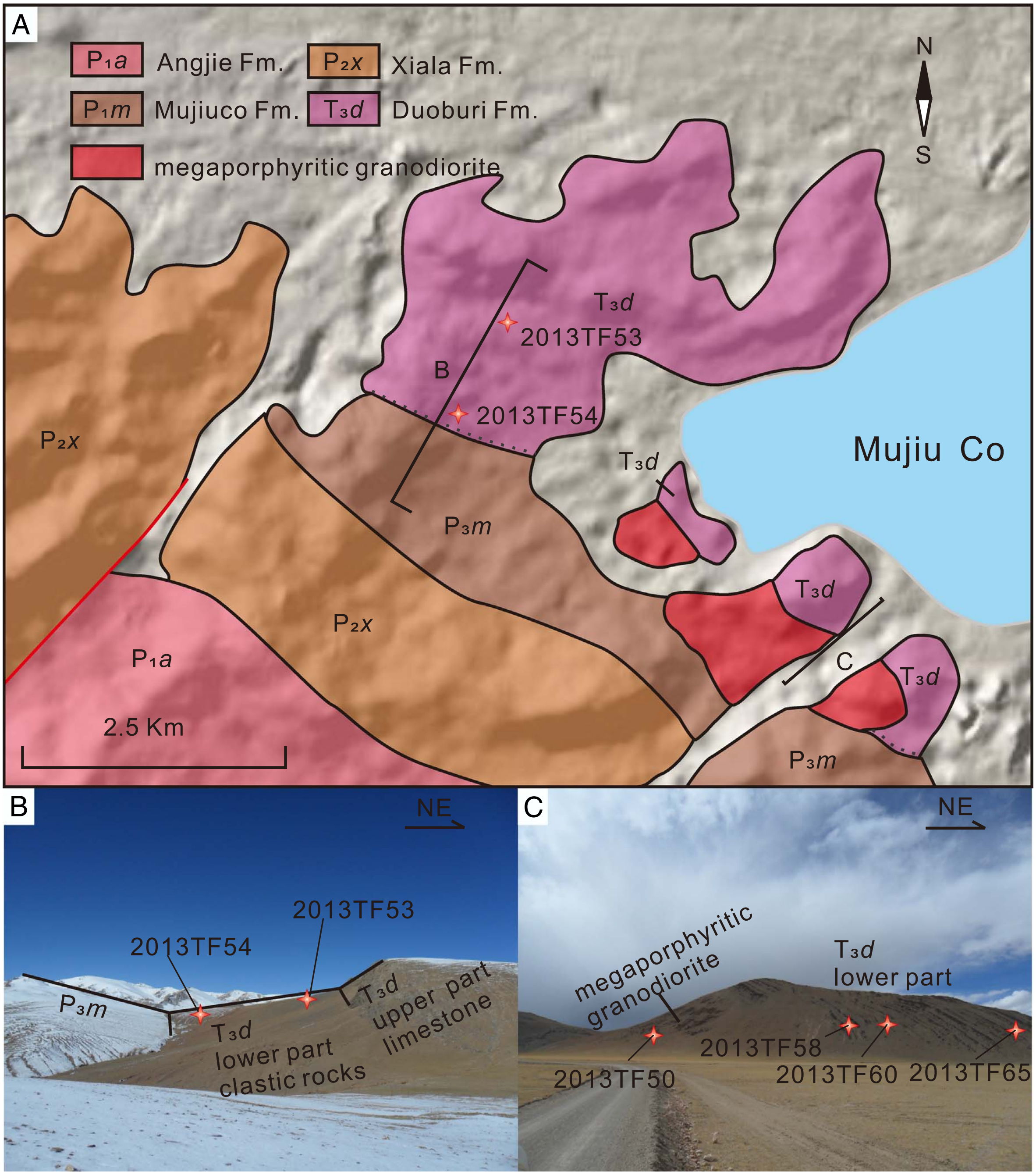


**Fig. 4.** (A) Geologic map of highlighting the distribution of Triassic sedimentary sequences to the west of Mujiu Co. (B) and (C) shows transects of Triassic strata and sample locations. The positions of the photographed transects are shown in (A).

### 3.6. Intermediate-felsic igneous rocks

In the mapped area, several intermediate-felsic igneous plutonic bodies crop out. The Rila Formation is intruded by a rhyolitic porphyry dike, which is in turn intruded by a potassium feldspar-rich dike. In the western portion of the mapped area, the rhyolite porphyry dike intrudes the Early Cretaceous Duoni Formation which contains interbedded andesitic volcanic rocks. In the central portion of the mapped area, black andesitic porphyry crops out. The phenocrysts consist of coarse-grained feldspars as large as 2 cm. The matrix mainly contains feldspar, amphibole, and quartz. In the southern portion of the study area, the Late Triassic Duoburi Formation is intruded by megaporphyritic granodiorite.

## 4. Structural geology

In the northern part of the Lhasa terrane, there are two laterally extensive east-west striking fault systems: the Gaize-Selin Co thrust system (GST) in the north and the Geren Co-Namu Co thrust system (GNT) in the south (Fig. 1B).

The GST is predominantly south-directed. It juxtaposes the Late Cretaceous Jingzhushan Formation, Cenozoic sediments, and minor Jurassic and Triassic strata in its hanging wall against Early Cretaceous sedimentary rocks in its footwall (Fig. 1B). Kapp et al. (2007a) propose that they are a series of back thrusts associated with the mainly south-directed thrust system along the Bangong-Nujiang suture, based on geologic relationships in the Nima area (Fig. 1A). In the Lunpola basin, Volkmer et al. (2014) proposed that north-directed thrusts, along with

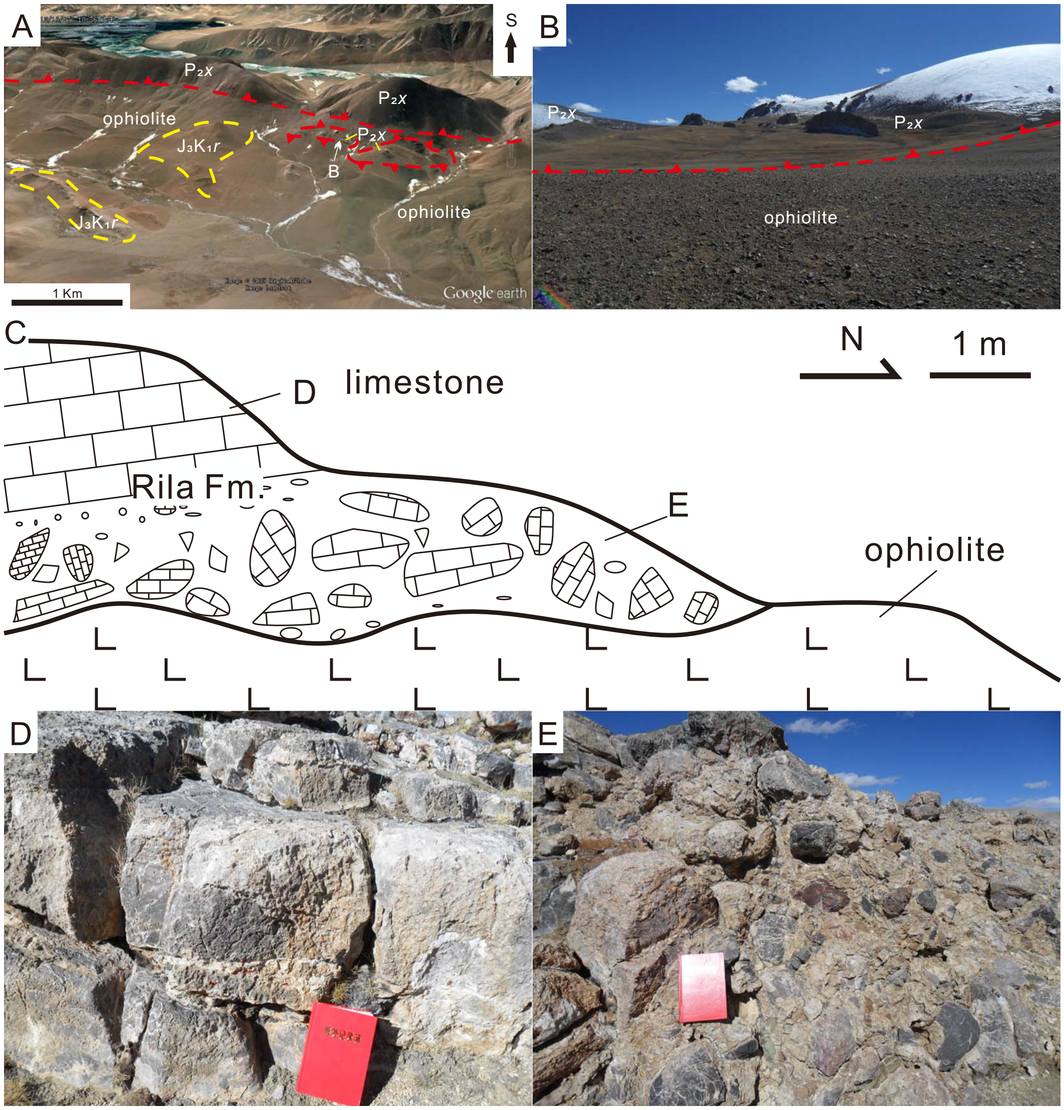


**Fig. 5.** (A) Google Earth views showing the spatial relationship between the Permian sequence, Rila Fromation, and Yongzhu ophiolites. (B) The north-directed thrust in (A) juxtaposes Permian strata in the hanging wall against ophiolitic rocks in the footwall. The position and view direction of the photo are shown as arrow in (A). (C) Sketch of an outcrop in (A) showing Rila Formation overlying the Yongzhu ophiolite. (D) and (E) are Rila Formation limestone in (C).

other north-directed thrust faults in the northern part of Lhasa terrane, near Coqin, (Murphy et al., 1997; Volkmer et al., 2007), are part of a passive roof thrust system.

The NW-SE striking GNT developed along the SNMZ. This thrust system juxtaposes Paleozoic strata in the hanging wall against Cretaceous sequences in the footwall. The Yongzhu ophiolite is also cut by this thrust system (Fig. 1B).

The mapped area covers a large part of the GNT. The northernmost thrust fault (F1 in Fig. 2) juxtaposes the Late Jurassic-Early Cretaceous Rila Formation in its hanging wall against the Early Cretaceous Langshan Formation in its footwall. This fault also cuts the rhyolite porphyry and potassium feldspar granite described above (Fig. 6D). F2 is subparallel to F1, cuts the Rila Formation, and juxtaposes the ophiolite in its hanging wall against the Rila Formation in its footwall (Fig. 6H, I). West of the mapped area, a NE-SW striking thrust fault (F3) cuts Cretaceous strata. F3 juxtaposes Cretaceous strata and the Rila Formation in its hanging wall against ultramafic rocks of the Yongzhu ophiolite in its footwall. The limestone of the Rila Formation and peridotite are locally deformed in an imbricate fan of north-directed thrusts (Fig. 6E, F). F3 also cuts the ophiolite and is overlain by the Cenozoic Wuyu group. Adjacent to F2, a red chert in the Rila Formation is brecciated (Fig. 6B). The Paleozoic strata in the southern portion of the mapped area are cut by several faults, and as a whole are displaced northward onto Cretaceous strata and the Yongzhu ophiolite by F4 (Fig. 5A, B). The ophiolite is locally overlain by the Rila Formation near the fault (Fig. 5). The western portion of F4 cuts the rhyolite that intrudes the Cretaceous Duoni Formation, and the central portion of F4 cuts the andesitic porphyry that intrudes the Paleozoic strata (Fig. 6G).

To the north of Geren Co, the GNT strikes NW-SE. It is north-directed and places the Paleozoic strata onto the Cretaceous sequence (Fig. 1B).

## 5. Petrography

Modal framework grain compositions of sandstone samples from the Xainza area were determined by point-counting standard thin sections, in order to identify potential provenance types. For each sample, > 360 grains were counted according to a modified Gazzi-Dickinson method, in which crystals larger than silt-sized within lithic grains are counted as monocrystalline grains (Dickinson and Suczek, 1979; Ingersoll and Suczek, 1979; Ingersoll et al., 1984). The modification was counting carbonate grains and tracking monocrystalline quartz grains that reside

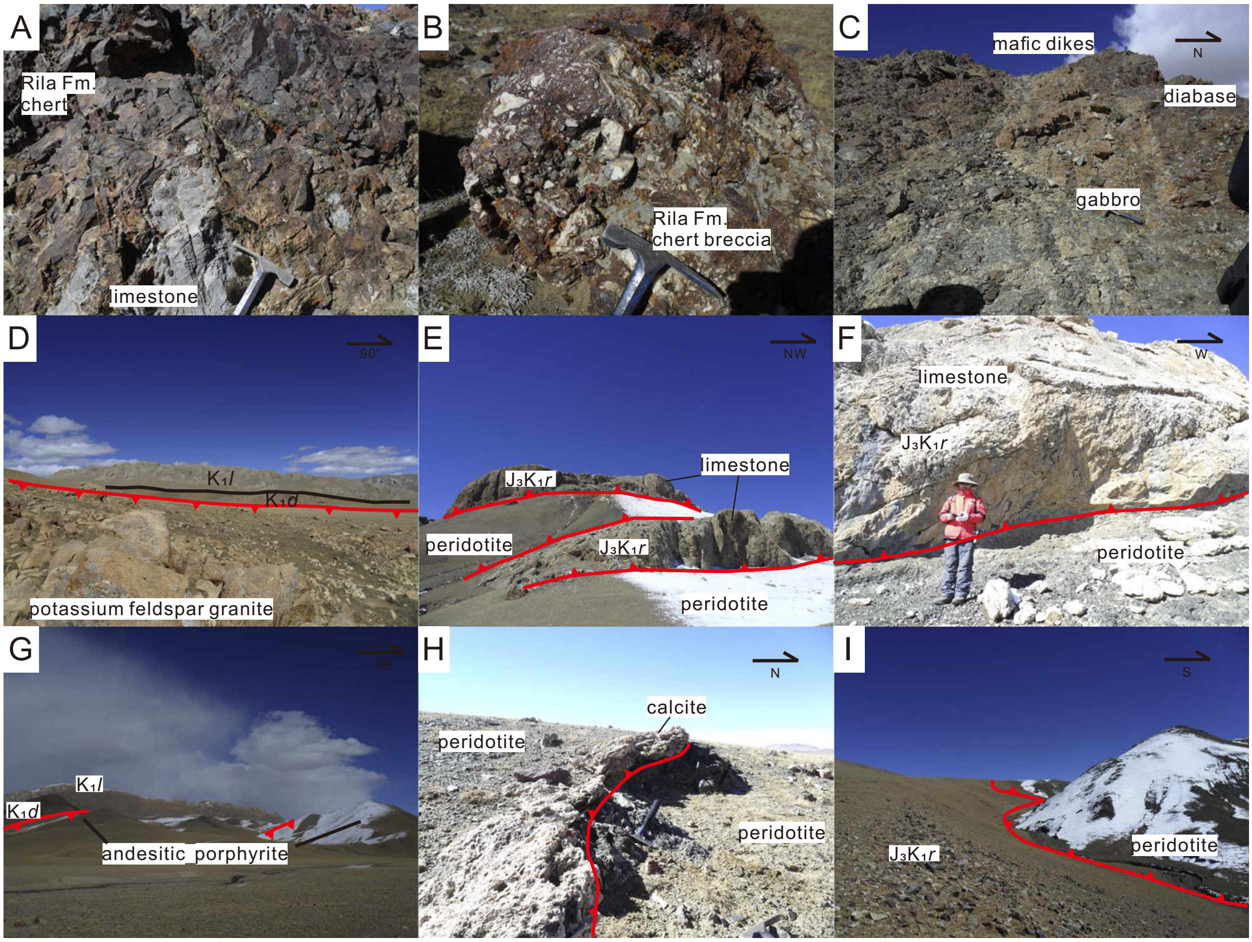


**Fig. 6.** (A) Rila Formation chert and limestone show poor bedding. (B) Breccia containing chert and limestone of Rila Formation at a thrust fault (F2 in Fig. 2) which juxtaposes the ophiolite northward onto the Rila Formation. (C) Mafic sheeted dike swarm. Sample location of 2013TF32. (D) The fault contact between felsic intrusions and Cretaceous strata. (E) North-directed imbricated fans containing the Rila Formation limestone and the Yongzhu ophiolites. (F) One of the thrust faults in the imbricated fan in (E). (G) Part of the fault F4 in Fig. 2. (H) The north-directed thrust in the ophiolite near the thrust in (I). (I) The north-directed thrust juxtaposes ophiolite onto Rila Formation (F2 in Fig. 2).

within quartzite-sandstone lithic grains (DeCelles et al., 2007). The six quantities calculated in thin sections were Qm (monocrystalline quartz), Qp (polycrystalline quartz), P (plagioclase feldspar), K (potassium feldspar), Lv (total volcanic lithic grains), and Ls (total sedimentary lithic grains). We calculate Qt = Qm + Qp, L = Lv + Ls, and Lt = L + Qp. 4 thin sections from Permian Angjie Formation, 4 thin sections from Triassic Duoburi Formation, and 2 thin sections from Cretaceous Duoni Formation were analyzed. The results are shown in Table 1 and plotted on ternary diagrams: Qp-Lv-Ls, Qt-F-L, and Qm-F-Lt. On Qp-Lv-Ls plots, the samples were well discriminated by tectonic setting (Fig. 8). On Qt-F-L plots, all plot in the recycled orogeny field. On Qm-F-Lt plots, the Permian Angjie Formation samples and Cretaceous Duoni Formation samples plot in the recycled orogeny field. The Triassic Duoburi Formation samples show affinity with the continental block field.

## 6. Zircon geochronology

### 6.1. U-Pb methods

Zircons for U-Pb dating were separated from 13 sandstones and 7 igneous rocks samples through traditional methods of crushing, grinding, and a combined method of flotation separation, magnetic separation, and heavy liquid separation techniques. Individual zircon grains were picked by hand under a binocular microscope. Zircons of each sample were randomly selected, mounted in epoxy resin and polished, in order to conduct U-Pb dating.

Zircons were analyzed using an Agilent 7500a ICP-MS coupled with a New Wave Research UP193FX Excimer at the Key Laboratory of Continental Collision and Plateau Uplift, Institute of Tibetan Plateau Research, Chinese Academy of Sciences, Beijing. The analytical procedures and the configuration of the LA-ICP-MS are described in Cai et al. (2012) and Ding et al. (2013). $^{206}Pb/^{208}U$ ages are taken as best ages if they are < 1000 Ma; otherwise, $^{207}Pb/^{206}Pb$ ages are taken as best ages. Zircon ages with a discordance of < 10% were considered to be usable. As for the igneous rocks, the usable ages generally have a younger cluster and few very older ones. We interpret the weighted mean age of the youngest cluster ($n \geq 3$) of zircon ages as the crystallization age, and the older zircon grains are interpreted as inherited grains. All uncertainties, including analytical and systematic, of the weighted mean ages are reported at the 95% confidence level. The weighted mean ages and probability density distribution were calculated and plotted by using ISOPLOT 3.0 of Ludwig (2003).

For the detrital zircon age data from Permian, Triassic and Cretaceous sandstones, normalized probability density plots were used to compare the different datasets. The Kolmogorov-Smirnoff (K-S) (Press et al., 1986) statistical test was used to assess the similarity of detrital zircon age populations among the samples. The returned $P$ value for each comparison represents the possibility that the two age distributions were drawn from the same population. When the $P$ value is larger than 0.05, it is of > 95% confidence that the two compared age populations are not statistically different.

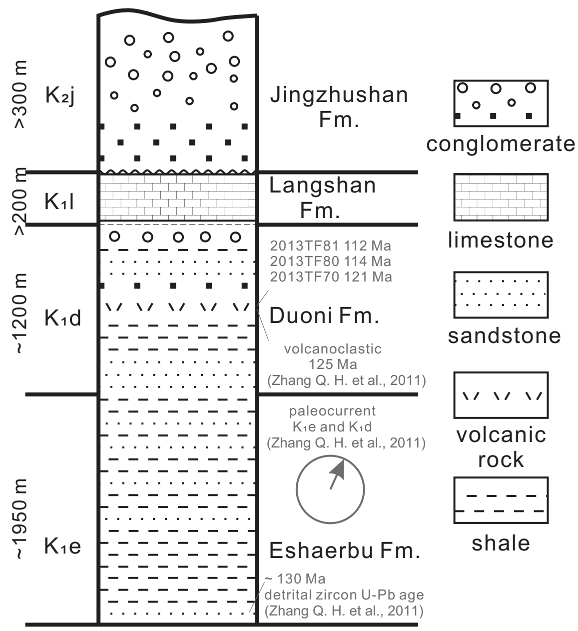


**Fig. 7.** A schematic column of composite stratigraphic sections of Cretaceous strata in Selin Co area (modified from Zhang et al., 2011). The ages of 2013TF81, 2013TF80, 2013TF70 are volcanic rock zircon U-Pb weighted mean ages (refer to Fig. 9 for details). Their positions shown in this stratigraphic column just indicate they are volcanic rocks in Duoni Formation, and do not mean they are collected from the same layer.

**Table 1**
Results of point-counting for the sandstone thin sections. In the table, Qt = Qm + Qp, L = Lv + Ls, Lt = L + Qp, total = Qm + Qp + Lv + Ls + F.

| Samples | Strata | Qm | Qp | Lv | Ls | F | Qt | L | Lt | In total |
|---|---|---|---|---|---|---|---|---|---|---|
| 2013TF14 | Permian | 252 | 41 | 33 | 26 | 53 | 293 | 59 | 100 | 405 |
| 2013TF13 | Permian | 269 | 30 | 41 | 24 | 76 | 299 | 65 | 95 | 440 |
| 2013TF87 | Permian | 236 | 33 | 28 | 13 | 64 | 269 | 41 | 74 | 374 |
| 2013TF91 | Permian | 293 | 38 | 16 | 9 | 102 | 331 | 25 | 63 | 458 |
| 2013TF65 | Triassic | 254 | 20 | 24 | 53 | 67 | 274 | 77 | 97 | 418 |
| 2013TF54 | Triassic | 229 | 12 | 20 | 15 | 85 | 241 | 35 | 47 | 361 |
| 2013TF53 | Triassic | 247 | 10 | 18 | 30 | 102 | 257 | 48 | 58 | 407 |
| 2013TF58 | Triassic | 244 | 28 | 31 | 17 | 111 | 272 | 48 | 76 | 431 |
| 2013TF84 | Cretaceous | 269 | 30 | 52 | 24 | 74 | 299 | 76 | 106 | 449 |
| 2013TF86 | Cretaceous | 251 | 26 | 30 | 70 | 85 | 277 | 100 | 126 | 462 |

To discuss the affinity of the Lhasa terrane, we compared the Permian data with previously published datasets from other areas. Since the Permian deposition was probably not directly sourced from the areas being compared (will be discussed below), K-S test will be too sensitive for any pair of the datasets to pass. Therefore, comparison of detrital zircon age datasets of Permian samples is also aided by multi-dimensional scaling (MDS) (e.g., Vermeesch, 2013; Saylor et al., 2017). MDS of detrital zircon data attempts to transform the dissimilarity between samples to distance in N-dimensional space. The misfit between the calculated distances and the disparities was represented by the "stress". In a low-stress MDS plot, the distances between points linearly correlate to the dissimilarities between samples. Dissimilarity was calculated as the coefficient of non-determination. For details about MDS, please refer to Vermeesch (2013) and Saylor et al. (2017).

### 6.2. U-Pb results

#### 6.2.1. Intrusive rocks

3 intermediate-felsic intrusive rocks were analyzed. The potassium feldspar granite 2013TF01 and megaporphyritic granodiorite 2013TF78 are cut by thrust faults (Fig. 2). The granite porphyry 2013TF50 intrudes the Triassic Duoburi Formation (Fig. 4). The zircons in these samples are mostly euhedral in morphology, and many of their CL images show zoning patterns. When calculating the weighted mean age of sample 2013TF50, two oldest ages in the used age cluster were rejected as they were far away from the average line and would make MSWD larger. The three samples yielded crystallization ages of 112.2 ± 0.6 (2013TF01), 105.1 ± 0.6 (2013TF50), 112.1 ± 0.6 Ma (2013TF78) (Fig. 9).

Only one sampled gabbro (2013TF32) yielded large enough zircons for U-Pb dating. The weighted average of the 27 zircons are 153.6 ± 2.3 Ma, which we interpret as the crystallization age of the mafic dikes (Fig. 9).

#### 6.2.2. Volcanic rocks

The volcaniclastic rock sample 2013TF70 collected from the Duoni Formation ($K_1$d) in the central part of the mapped area (Fig. 2) yielded a crystallization age of 121.0 ± 0.7 Ma (Fig. 9). One rhyolite sample (2013TF80) and one andesite sample (2013TF81) were collected from the transect (TS3) north of Geren Co in Cretaceous strata (Fig. 1B). They yielded crystallization ages of 113.6 ± 0.7 Ma and 112.2 ± 0.6 Ma, respectively (Fig. 9).

#### 6.2.3. Sandstones

13 sandstone samples were collected from Permian, Triassic, and Cretaceous strata, and 100 zircon grains were analyzed from each sample.

*6.2.3.1. Permian.* 6 Permian sandstone samples were analyzed. The

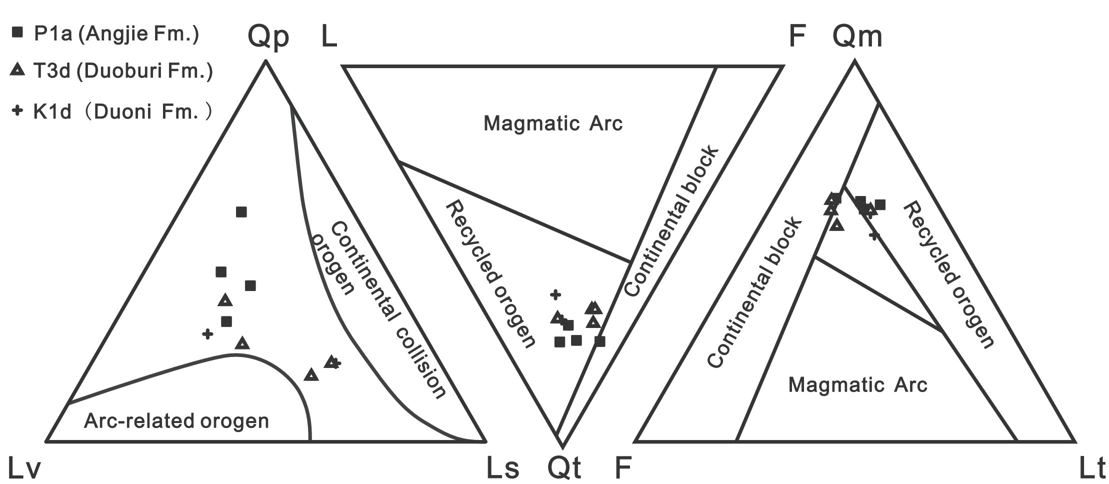


**Fig. 8.** Ternary diagrams showing modal framework compositions of sandstone grains in the Angjie Formation, Duoburi Formation, and Duoni Formation.

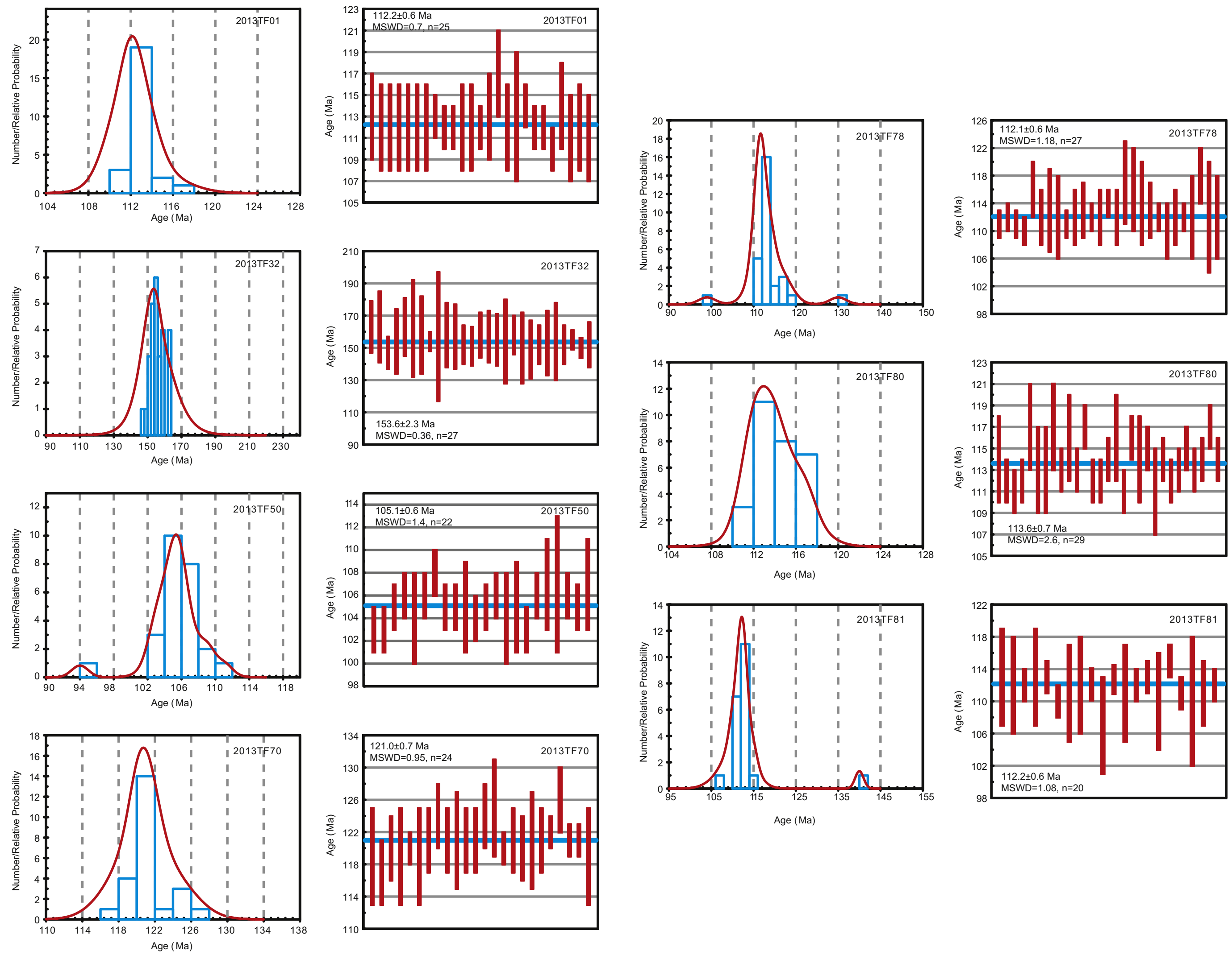


**Fig. 9.** U-Pb relative age probability density plots of analyzed igneous rocks from this study, and their weighted mean ages. Uncertainties are reported at the 95% confidence level.

normalized age probability density plots of all the detrital zircons are shown in Fig. 10A

Sample 2013TF13 and 2013TF16 were collected from transect TS1 in the Angjie Formation (Fig. 1B). The sandstone bed containing 2013TF13 is coarse-grain and partly contains conglomerates. 2013TF16 is a gray-white quartz sandstone. The probability density plots of 2013TF13 and 2013TF16 are similar. Grain ages range from 457 Ma to 3398 Ma. Sample 2013TF20 is a fine-grain sandstone from the Angjie Formation. This sample only yielded 38 usable ages. The youngest age is 743 Ma, much older than the youngest ages from other analyzed Permian samples, which may be a result of the small population of grains analyzed. Sample 2013TF87, 2013TF89, and 2013TF91 were collected from different layers of gray-white low-grade metasandstone in transect TS2 in the Angjie Formation (Fig. 3). U-Pb zircon ages primarily range from 500 to 2700 Ma (Fig. 10A).

479 usable ages in total were yielded from 6 samples in the Angjie Formation. The majority of the ages range from 500 Ma to 2000 Ma. They show two large populations of ages from 457 to 640 and from 892 to 998 Ma. Between the two ranges, the ages are also distributed with a less dominant population at 800–850 Ma. In the order of prominence, there are also age groupings of 1000–1350 Ma (peak of 1100 Ma), 1500–1800 Ma (peak of 1600 Ma), and 2350–2650 Ma (peak of 2450) (Fig. 10A).

*6.2.3.2. Triassic*. 4 Triassic sandstone samples collected from the lower part of the Duoburi Formation west of Mujiu Co were analyzed. The relative probability plots of all the detrital zircons ages are shown in Fig. 10B.

2013TF53 is coarse sandstone with thin beds of conglomerate. 2013TF54 is gray-white quartz sandstone, collected from just above the unconformity between the Triassic Duoburi Formation and Permian limestone. 2013TF60 and 2013TF65 were collected from beds interbedded with bioclastic limestone and wacke (Fig. 4). The age distribution patterns of the detrital zircons of the 4 samples are similar. 336 usable ages in total were yielded from the 4 samples. The majority of the ages are from 500 Ma to 2000 Ma. Only 2 ages are < 450 Ma, which are 356 ± 3 Ma and 405 ± 3 Ma. Grains with ages between 450 and 650 Ma are the most prominent, with a peak at 500 Ma. A wide age cluster exists between 850 and 1250 Ma, with two secondary clusters at 900–1000 Ma and 1050–1200 Ma. The remaining ages are mainly in clusters between 1450 and 1700 Ma and 2350–2700 Ma (Fig. 10B).

*6.2.3.3. Cretaceous*. Sample 2013TF74 is a gray-white sandstone, collected from the Duoni Formation in the western portion of the mapped area. Sample 2013TF84 and 2013TF86 were collected from transect TS3, the upper part of the Duoni Formation. The probability plots of all of the detrital zircons are shown in Fig. 10C.

233 usable ages were yielded from the 3 samples. The most prominent age cluster is 113–146 Ma (peak at ca. 124 Ma). A less

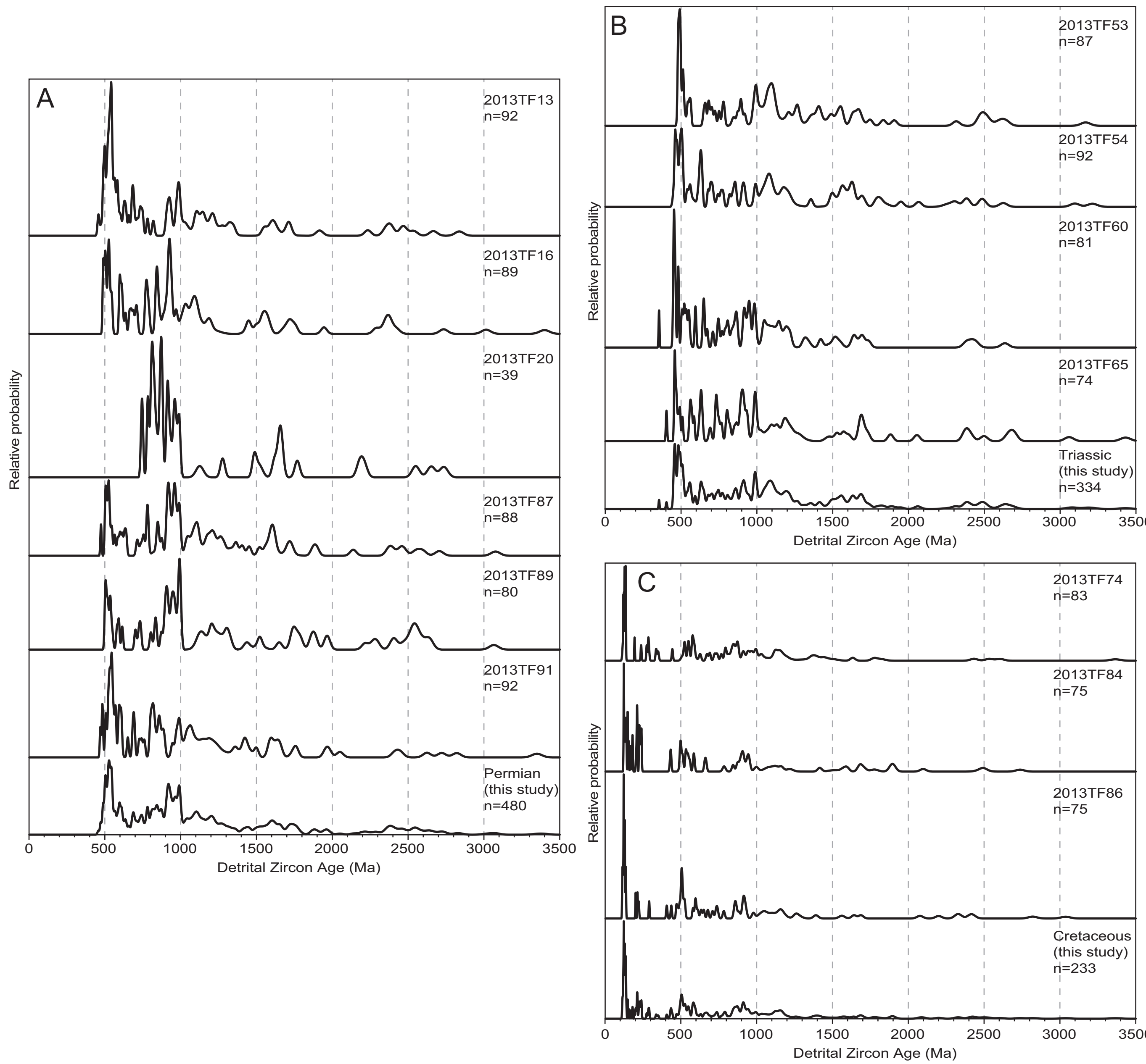


**Fig. 10.** Normalized U-Pb age probability density plots of the samples from Permian Angjie Formation (A), Triassic Duoburi Formation (B), and Cretaceous Duoni Formation (C). The bottom panel of each column shows the whole data from that formation.

prominent age cluster is 205–239 Ma, which is mainly contributed by sample 2013TF84. The remaining ages are older than 400 Ma, in clusters of 400–600 Ma, 800–1000 Ma, and 1050–1200 Ma (Fig. 10C).

## 7. Discussion

### 7.1. The affinity of the Lhasa Terrane

In order to assess the affinity of Lhasa terrane, the age distribution pattern of detrital zircons from Permian samples in the Lhasa terrane was compared with age data from Northern Qiangtang, Southern Qiangtang, Australia, Tethyan Himalaya, High Himalaya, and Lower Himalaya (Fig. 11A). The Southern Qiangtang, Tethyan Himalaya, High Himalaya, and Lower Himalaya are widely thought to represent material from Indian Gondwanan (e.g. Yin and Harrison, 2000; Gehrels et al., 2011; Zhu et al., 2011a). Many researchers also think the Northern Qiangtang terrane also rifted from India before it was accreted to Asia (Yin and Harrison, 2000). The data are from Cawood and Nemchin (2000), Veevers et al. (2005), Leier et al. (2007c), Aikman et al. (2008), Pullen et al. (2008b, 2011), Dong et al. (2011), Gehrels et al. (2011), and references therein, Webb et al. (2011, 2013), Zhu et al. (2011a).

The 457–640 Ma zircon grains are prominent in Northern Qiangtang, Southern Qiangtang, Western Australia, and Tethyan Himalaya (Fig. 11A). The 800–850 Ma zircons grains are compatible with the small age peaks in Qiangtang, and are also compatible with the relative high plateau in the age-probability curve of Tethyan Himalaya and High Himalaya, but is absent in Western Australia (Fig. 11A). In this study, the age group of 900–1000 Ma is more prominent than the group of 1000–1350 Ma, which is opposite to the result of Zhu et al. (2011a), but is compatible with that of Southern Qiangtang and Tethyan Himalaya (Fig. 11A). Zhu et al. (2011a) suggested that the 1170 Ma peak in Lhasa terrane indicates an Australian source. Although we also got a comparable cluster (1000–1350 Ma) in this study, they

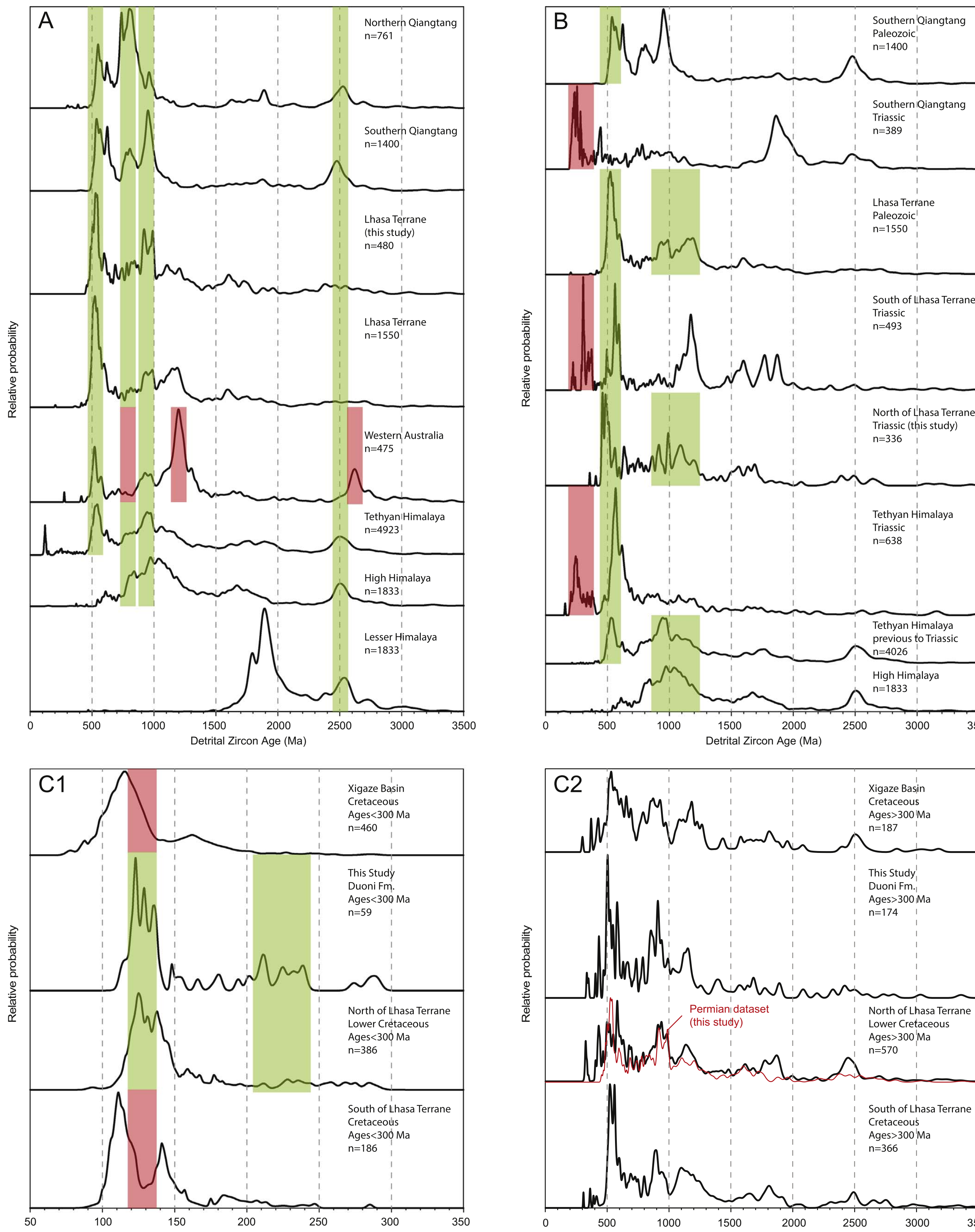


**Fig. 11.** Comparison of the normalized U-Pb zircon age probability density plots of the (A) Permian, (B) Triassic, and (C) Cretaceous samples with previously published datasets. For the comparison of Cretaceous samples (C), the left panel displays the ages younger than 300 Ma, and the right panel displays the ages older than 300 Ma. Refer to text for source of comparison datasets.

may indicate affinity with Tethyan Himalaya and High Himalaya as zircons of a wide age span from 800 to 1350 Ma are predominant there (Gehrels et al., 2011). Integrating previously published data from the Lhasa terrane with our results shows two comparable age groups at 900–1000 Ma and 1050–1250 Ma (Fig. 11A). This feature correlates with the wide age span from 800 to 1350 Ma of the Tethyan Himalaya and High Himalaya. The age group of 1500–1800 Ma (peak of 1600 Ma) correlates well with the age-probability curves of Tethyan and High Himalaya. The age group of 2350–2650 Ma (peak of 2450 Ma) is also prominent in Qiangtang and Himalaya, which correlates poorly to the curve of Australia (Fig. 11A). This age group in Lhasa terrane is not as prominent as in Himalaya and Qiangtang. The reason could be the lack of exhumation of the oldest Precambrian basement. As we mentioned in the geological setting section, the Northern and Southern Lhasa subterranes are mainly juvenile crusts which do not have much Precambrian basement, and the narrow Central Lhasa terrane, which contains Precambrian basement, is covered by complete Paleozoic sequence from Cambrian to Permian.

To test this interpretation, K-S tests was done for our Permian samples, compiled dataset (including the data in this study) of Paleozoic strata in the Lhasa terrane, Western Australia, Tethyan Himalaya and Southern Qiangtang. Neither our data and compiled data of Lhasa terrane passed the K-S tests with any of the Western Australia, Tethyan Himalaya and Southern Qiangtang (Table 2). This could be because the dated samples are mainly Carboniferous and Permian, and their material could be recycled material within the Lhasa terrane and was not directly sourced from Indian or Australia. Studies indicate that, in Paleozoic, the Lhasa terrane started rifted from the Gondwana as early as Devonian and was an isolated block in the Paleo-Tethyan Ocean by Permian (Zhu et al., 2010, 2013). The other possible reason is that the K-S test is too sensitive to be used in comparing the affinity of two large terranes. The failure in the K-S test simply means that it is not of 95% confidence that the compared datasets are statically the same.

To statically compare the relative similarity between these datasets, multidimensional scaling (MDS) was conducted (Fig. 12). In the 3D MDS plot (left panel) in Fig. 12, the red solid lines and the black dash lines point from each sample to its closest neighbor and second closest neighbor respectively. The Shepard plot (right panel) shows the distances in the MDS can represent dissimilarities between the datasets well (stress is low, 0.12487). The MDS shows that, for all our analyzed samples, their closest or second closest neighbor is Tethyan Himalaya or Southern Qiangtang. No arrow in the plot points from our samples to the Western Australia.

Both the probability density plots and the MDS show that the age distribution of the Paleozoic strata in the Lhasa terrane is more similar to Tethyan Himalaya and Southern Qiangtang than Western Australia. This indicates that the source of detrital material was of high affinity with Indian Gondwana. This further suggests that the Lhasa terrane rifted away from the northern margin of Indian plate before it collided with the Qiangtang terrane to the north (Allégre et al., 1984; Leeder et al., 1988; Pearce and Mei, 1988; Yin and Nie, 1993; Metcalfe, 1996; Yin and Harrison, 2000), and not from Australia as Zhu et al. (2011a) proposed.

### 7.2. Sediment provenance of Triassic strata and its implication

U-Pb detrital zircon ages of Triassic Duoburi Formation are compared with data from Southern Qiangtang, Southern Lhasa Terrane, and Tethyan Himalaya. The detrital zircon ages from the Duoburi Formation in the Xainza area lacks ages younger than 450 Ma (only two grains of 356 Ma and 405 Ma respectively) (Fig. 11B). Contemporary strata in the Qiangtang terrane and BNSZ, South part of the Lhasa terrane, and the Tethyan Himalaya have an age cluster of 200–350 Ma (Aikman et al., 2008; Li et al., 2010, 2014a; Gehrels et al., 2011; Webb et al., 2013; Cai et al., 2016; Li et al., 2017). It should be noticed that the age-probability curve of samples from the Duoburi Formation in the Xainza area is very similar to the curve of Paleozoic strata in the Lhasa terrane. Both of them have age groups at 470–550 Ma, 900–1000 Ma, 1050–1200 Ma, 1450–1700 Ma, and 2350–2700 Ma (Fig. 11B). This is also confirmed by the K-S test. Each of our Triassic samples and the

**Table 2**
*P*-values from Kolmogorov-Smirnov (K-S) tests of detrital-zircon ages using error in the cumulative distribution function (CDF).

| Permian data | Angjie Fm. | Lhasa | Australia | Tethyan Himalaya | Southern Qiangtang |
|---|---|---|---|---|---|
| Angjie Fm. | – | **0.083** | 0.000 | 0.000 | 0.000 |
| Lhasa | **0.083** | – | 0.000 | 0.000 | 0.000 |
| Australia | 0.000 | 0.000 | – | 0.000 | 0.000 |
| Tethyan Himalaya | 0.000 | 0.000 | 0.000 | – | 0.000 |
| Southern Qiangtang | 0.000 | 0.000 | 0.000 | 0.000 | – |

| Triassic data | 2013TF53 | 2013TF54 | 2013TF60 | 2013TF65 | Duoburi Fm. | Angjie Fm. |
|---|---|---|---|---|---|---|
| 2013TF53 | – | **0.780** | 0.040 | **0.440** | **0.453** | **0.107** |
| 2013TF54 | **0.780** | – | **0.170** | **0.901** | **0.915** | **0.254** |
| 2013TF60 | 0.040 | **0.170** | – | **0.562** | **0.355** | **0.191** |
| 2013TF65 | **0.440** | **0.901** | **0.562** | – | **0.981** | **0.845** |
| Duoburi Fm. | **0.453** | **0.915** | **0.355** | **0.981** | – | **0.067** |
| Angjie Fm. | **0.107** | **0.254** | **0.191** | **0.845** | **0.067** | – |

| Cretaceous data | 2013TF74 | 2013TF84 | 2013TF86 | Duoni Fm. (> 300 Ma) | Angjie Fm. | Duoburi Fm. |
|---|---|---|---|---|---|---|
| 2013TF74 | – | **0.322** | **0.731** | 0.005 | 0.000 | 0.001 |
| 2013TF84 | **0.322** | – | **0.781** | 0.000 | 0.000 | 0.000 |
| 2013TF86 | **0.731** | **0.781** | – | 0.003 | 0.000 | 0.001 |
| Duoni Fm. (> 300 Ma) | 0.005 | 0.000 | 0.003 | – | **0.338** | **0.193** |
| Angjie Fm. | 0.000 | 0.000 | 0.000 | **0.338** | – | **0.075** |
| Duoburi Fm. | 0.001 | 0.000 | 0.001 | **0.193** | **0.075** | – |

P values in bold are > 0.05.

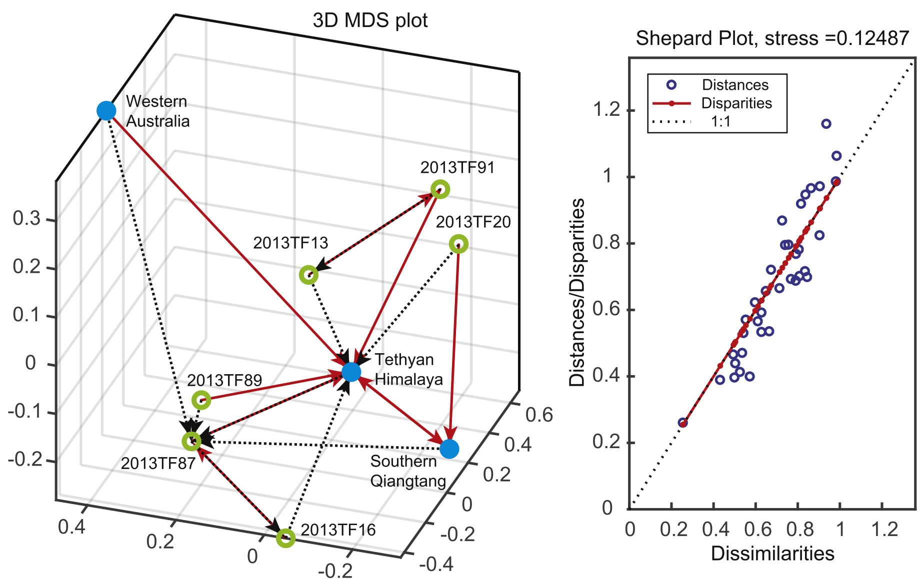


**Fig. 12.** 3-dimensional multidimensional scaling plot of the Permian Angjie Formation samples (green circles), Tethyan Himalaya, Southern Qiangtang, and Australia datasets (blue solid dots). Dissimilarity is based on the complement of the cross-correlation coefficient. The red solid lines and the black dash lines in the MDS plot (left panel) point from each sample to its closest neighbor and second closest neighbor respectively. (For interpretation of the references to color in this figure legend, the reader is referred to the web version of this article.)

compiled data passed the K-S test with the Permian data (Table 2), which indicates that the age distributions of each Triassic sample and the compiled data are of > 95% confidence statically the same as Permian data.

The outstanding difference in the age-probability curve between Southern Qiangtang and Duoburi Formation indicates almost no material in Duoburi Formation was derived from Southern Qiangtang. This is compatible with the suggestion that the Bangong-Nujiang ocean had not closed by that time (Girardeau et al., 1984; Pearce and Deng, 1988; Shi et al., 2004; Zhang et al., 2012; Zhang Y. X. et al., 2007a; Baxter et al., 2009; Liu et al., 2014; Fan et al., 2015; Zeng et al., 2016; Wang et al., 2016a; Li et al., 2017).

Different from the scarcity of the Triassic strata in the Northern Lhasa terrane, Triassic sequences widely outcrop in the south part of the Lhasa terrane. Li et al., 2010; 2014a) suggested that the supply of detritus to Triassic strata in Southern Lhasa and part of the Tethyan Himalaya was associated with a recently proposed Late Permian-Early Triassic orogenic event along the LMF (Fig. 1A). The orogenic event is recorded by Late Permian-Early Triassic high and ultra-high pressure metamorphism (Chen et al., 2009; Li et al., 2003; Yang et al., 2009; Dong et al., 2011; Li et al., 2011) and contemporary magmatism (Kapp et al., 2005). In the Southern Lhasa terrane, Permian and Triassic igneous rocks are widely exposed (Li et al., 2003; Zheng et al., 2003; Kapp et al., 2005; Chu et al., 2006; He et al., 2006a; Liu et al., 2006; Zhang Y. X. et al., 2007a; Zhu et al., 2009, 2011b, 2013). However, this orogenic event and contemporary magmatism are unlikely to have contributed to the Duoburi Formation in the Xainza area, as Duoburi Formation lacks detrital zircons of age groups of 200–350 Ma. Furthermore, the Duoburi Formation sandstone is interbedded with wacke, and most sandstone beds are coarse-grained and contain angular clasts, suggesting that they have a proximal source. Therefore, we interpret the provenance of Duoburi Formation is the proximal Paleozoic strata (mainly Carboniferous and Permian) in Xainza area, which is different from that of the contemporary strata in Southern Qiangtang, south part of the Lhasa terrane and Tethyan Himalaya.

### 7.3. The tectonic nature of Yongzhu ophiolite

The age of the Yongzhu ophiolite is not well-constrained. One 139 Ma K-Ar age from a pillow basalt was reported by Wang et al. (2003). Zircon U-Pb ID-TIMS dating results show that three zircon grains from a diabase range from ca. 114 to 133 Ma (Zhu, 2004) and one grain from a gabbro dike is 178 ± 10 Ma (Qu et al., 2011). The depositional age of the radiolarian chert is constrained to be Late Jurassic-Early Cretaceous (Qu et al., 2003b). In this study, we obtained a U-Pb weighted mean age of 27 zircon grains as 153.6 ± 2.3 Ma. We interpret this Late Jurassic age as the formation time, or at least in part, of the Yongzhu ophiolite.

There are other ophiolites distributed along the SNMZ. Geochronologic and paleontologic results show that they mainly formed from Middle Jurassic to Early Cretaceous (Tang et al., 2004; Ye et al., 2004; Zhang Y. X. et al., 2007a; Xu et al., 2014; Zhong et al., 2015). In some areas, such as Bomi, Namu Co, Ren Co, Gaize, and Shiquanhe, ophiolites are estimated to have formed as early as Late Triassic to Early Jurassic (He et al., 2006b; Zheng et al., 2006; Fan et al., 2010; Zhong et al., 2015). Geochemistry studies of the ophiolites in this belt, including the Yongzhu Ophiolite, suggest that they were generated in a back-arc basin or intra-arc basin setting (Qiu et al., 2007; Wang et al., 2007; Xu et al., 2014; Zhong et al., 2015).

A dispute regarding the ophiolites along the SNMZ is whether they represent another suture within Lhasa terrane or are translated southwards in thrust sheets rooted into the BNSZ. The similarity of lithological and structural characteristics of the Dongqiao and Yongzhu ophiolites suggested to Girardeau et al. (1984, 1985) that they are translated as thrust sheets rooted into the BNSZ. Coward et al. (1988) supports this viewpoint by based on the geometry and kinematics of the structures and their relationship with the tectonostratigraphy along the BNSZ and Xainza area. In the Shiquanhe area, Kapp et al. (2003a) also interpret the ophiolites as thrust sheets that root into the BNSZ. We find that this model has the following shortcomings:

First, the Yongzhu ophiolite is about 200 km south of the BNSZ (Fig. 1A), and the BNSZ and adjacent areas experienced large amount (> 50%) of north-south shortening since Mesozoic (Murphy et al., 1997; Kapp et al., 2003a, 2007a; Volkmer et al., 2007, 2014). Therefore, if Yongzhu ophiolite is within thrust sheets from BNSZ, the total amount of southward thrusting should exceed 300 km. This large amount of movement requires associated large-scale south-directed thrust faults that transport the ophiolites thrust sheet southward across the Selin Co basin. However, most of the documented south-directed thrusts that accommodate the shortening are locally distributed along the BNSZ along the north side of the Selin Co basin while the Yongzhu ophiolite is located along the south side of the basin and bounded by north-directed thrusts.

Second, the Dongqiao ophiolite, the closest ophiolite in BNSZ to the Yongzhu ophiolite, is overlain by Jurassic strata. Similarly, the Yongzhu ophiolite is overlain by the Late Jurassic-Early Cretaceous Rila

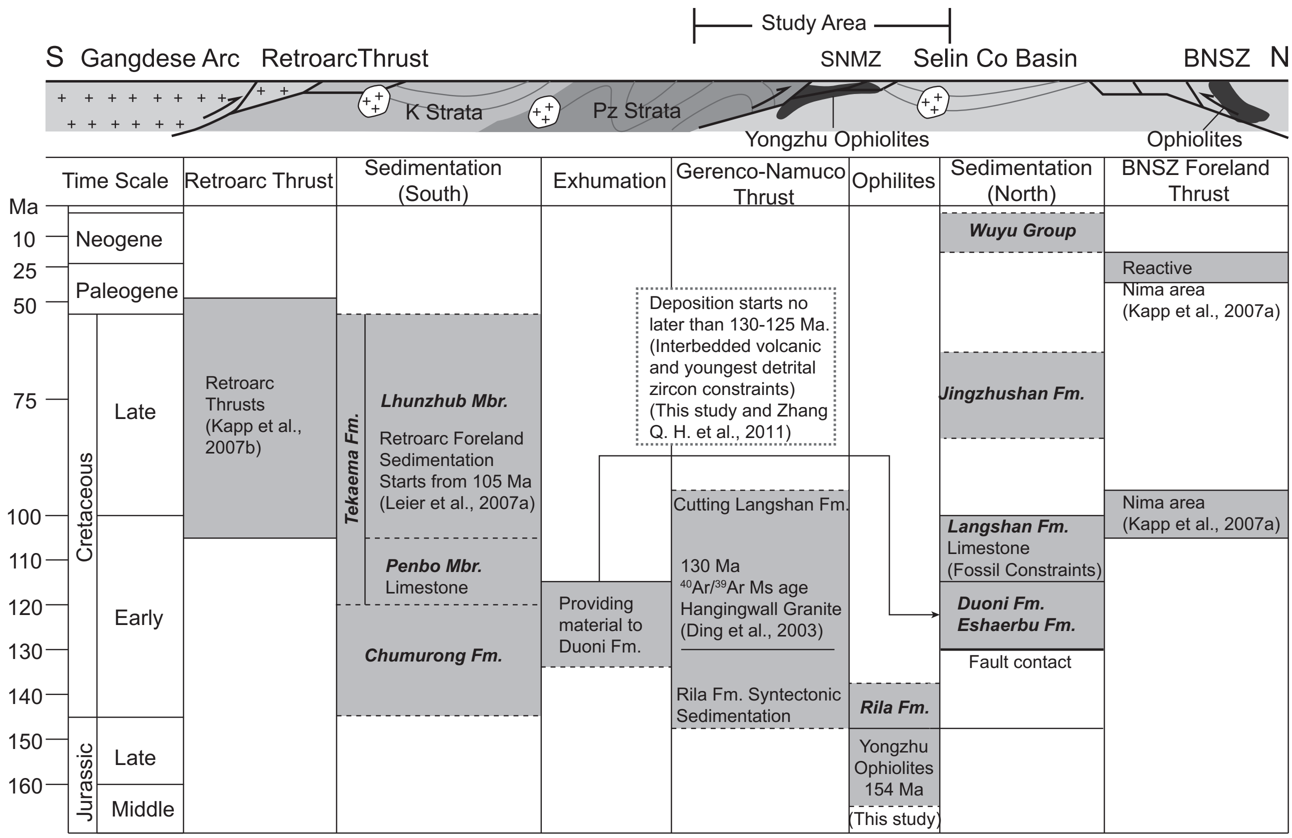


**Fig. 13.** Summary of Late Jurassic to Neogene tectonic events in Lhasa terrane. The schematic cross section of Lhasa terrane shows the relative positions of the events in the chart below it. Notice that the exhumation of the Paleozoic strata, deposition of the Cretaceous strata, and activation of the Geren Co-Namu Co thrust are earlier than the Gangdese retroarc thrust system and the foreland thrusts in BNSZ. The dash lines in the chart mean the time estimates are not well-constrained.

Formation. These observations indicate emplacement occurred before Late Jurassic (Fig. 13). However, geologic mapping, U-Pb zircon geochronology and thermochronologic data including $^{40}Ar/^{39}Ar$ K-feldspar, muscovite and, biotite dating and apatite fission track and apatite (U-Th)/He dating show that slip along south-directed thrusts in BNSZ were active after the late stages of the Early Cretaceous (Kapp et al., 2003a, 2007a; Volkmer et al., 2007, 2014) (Fig. 13).

Third, if large scale shortening occurred between the BNSZ and Xainza area, there should be associated geological effects, such as thickening of the lithosphere, the exhumation of older strata (or even basement), and surface uplift between them. However, the Selin Co and Lunpola areas between the BNSZ and SNMZ have been large sedimentary basins since Early Cretaceous, just after the emplacement of the Yongzhu ophiolite (Fig. 13).

Therefore, the Yongzhu ophiolite is less likely to be translated southwards in a thrust sheet rooted in the BNSZ. We envision that the Yongzhu ophiolite represents a separate suture zone from the BNSZ within the Lhasa terrane. It and other ophiolites along the SNMZ may also represent remnants of an oceanic basin which existed between the Northern and Central Lhasa terranes during Jurassic.

### 7.4. Cretaceous tectonic evolution

#### 7.4.1. Sediment provenance of Lower Cretaceous strata in Selin Co Basin

To investigate the provenance of the Lower Cretaceous strata in Selin Co basin and Lunpola basin in the northern Lhasa terrane and its differences from contemporary strata in the retroarc foreland basin and the forearc basin, we compare the age-probability curves of the Duoni formation (data in this study), the Cretaceous strata in the Selin Co basin and the adjacent Lunpola basin in the north of Lhasa terrane, the Takena formation in Linzhou basin (retroarc foreland basin) in Lhasa area, and the early Cretaceous forearc strata in the Xigaze basin (Fig. 11C). The data are from Leier et al. (2007a, 2007b), Pullen et al. (2008a), Wu et al. (2010), Aitchison et al. (2011), Zhang Q. H. et al. (2011a), and Volkmer et al. (2014).

The Cretaceous data have few ages from 300 to 400 Ma, and the ages < 300 Ma are predominant over ages larger than 400 Ma. The age-probability curve of zircons older than 400 Ma is very similar to those of the Paleozoic strata and Triassic strata in the Central Lhasa terrane (Fig. 11C). This is also confirmed by the K-S test results. The older portion (> 300 Ma) of the compiled data from Cretaceous samples past the K-S test with both Permian dataset and Triassic dataset acquired in this study (Table 2). As for the zircons younger than 300 Ma, both the north and south part of the Lhasa terrane have a predominant age group between 105 and 145 Ma, which is likely due to the extensive magmatic activities in the Lhasa terrane during the Early Cretaceous (Ji et al., 2009a; Zhu et al., 2013, 2016). The detrital zircon ages from the Duoni Formation have an age peak cluster at 120–140 Ma (Fig. 11C). Igneous rocks in this time span are extensively exposed in the north part of the Lhasa terrane (Kapp et al., 2007a; Volkmer et al., 2007, 2014; Zhu et al., 2009, 2011b, 2016; Gao et al., 2011). However, in the south part of Lhasa terrane and Xigaze basin, this peak is absent, although igneous rock in this time span exists (Zhu et al., 2013; Wang et al., 2017). Instead, the predominant age peak clusters in the south part of the Lhasa terrane are at 105–125 Ma and 140–145 Ma, and in the Xigaze basin at 100–125 Ma (Fig. 11C). Their provenance is interpreted as the Gangdese magmatic belt. In south Lhasa terrane, Early Cretaceous strata have a less predominant cluster between 175 and 200 Ma, which is absent in the Northern Lhasa terrane (Fig. 11C). These strata may be sourced from the Gangdese magmatic arc and volcanic rocks in Yeba Formation which contain large amount of Late Triassic-Jurassic igneous rocks (Li et al., 2003; Chu et al., 2006; Dong et al., 2006; Geng et al., 2006; Zhang H. F. et al., 2007b; Zhu et al., 2008; Ji et al., 2009b; Guo et al., 2013; Song et al., 2014; Kang et al., 2014; Meng et al., 2015; Wang et al., 2016b). Moreover, Early Cretaceous strata contain a small group of detrital zircons of 200–240 Ma, which are less dominant in the Xigaze basin and the south portion of the Lhasa terrane (Fig. 11C). As zircons of this time span are common in Mesozoic strata and igneous and metamorphic rocks along the BNSZ and the Qiangtang terrane (Fig. 11B) (Kapp et al., 2003b; Pullen et al., 2008b; Li et al., 2009; Li et al., 2011; Fu et al., 2010; Gehrels et al., 2011; Liang et al., 2012; Zhai et al., 2013; Fan et al., 2015; Zeng et al., 2016), we suggest they are the source of the 200–240 Ma zircons in Northern Lhasa terrane. Therefore, we infer that the source of the Duoni Formation in Northern Lhasa is primarily Cretaceous igneous rocks and Paleozoic strata in the Northern and Central Lhasa terrane, as well as some input from the BNSZ and Southern Qiangtang, with little material sourced from Gangdese arc. This is compatible with the paleo-flow estimates showing sediment transport via north and south-directed streams (Zhang Q.H. et al., 2011a; Leier et al., 2007b).

#### 7.4.2. Tectonic setting

Zhang et al. (2012) suggested that the Lhasa terrane experienced a period of extension during the Cretaceous based on geochemistry data from contemporary igneous rocks in the north part of Lhasa terrane and occurrence of a marine transgression recorded by regional carbonate deposition (Langshan Formation). The roll-back of the Neo-Tethyan oceanic lithosphere is considered to be the cause of a back-arc extensional setting (Fig. 14A). However, no south-north extensional structures supporting this model have been recognized. On the contrary, many observations indicate that large amount of north-south shortening was accommodated by folding and thrusting in Lhasa terrane in Cretaceous (Kapp et al., 2003a, 2007a; Volkmer et al., 2007, 2014; Murphy et al., 1997; Pullen et al., 2008a; He et al., 2007). In Xainza area, Early Cretaceous igneous rocks, such as 112 Ma potassium feldspar granite (2013TF01) and 112 Ma andesitic porphyrite (2013TF78), are cut by thrust faults, which are overlain by undeformed Neogene conglomerate and sandstone (Fig. 2). Studies of Cretaceous strata sequence in the Northern Lhasa terrane indicated they are foreland basin type (DeCelles et al., 2007; Leier et al., 2007a; Zhang Q. H. et al., 2011a). In addition, petrographic observations indicate the provenance of Cretaceous was a recycling orogeny setting (Zhang Q. H. et al., 2011a; this study) (Fig. 8).

Although it is clear that the Lhasa terrane experienced shortening during the Cretaceous, the causes are still unclear. Previous mapping results in other areas, interpret the north-directed thrusts in the north part of the Lhasa terrane as back thrusts or passive roof thrusts of the primarily south-directed foreland thrust belt along the BNSZ (Murphy et al., 1997; Kapp et al., 2007a; Volkmer et al., 2007, 2014) (Fig. 14B). Therefore, the Cretaceous basins south of the BNSZ in the Northern Lhasa terrane were correspondingly interpreted as peripheral foreland basins with sediment sources along the BNSZ or Qiangtang and with minor sediment input from the Lhasa terrane (Fig. 14B). Alternatively, Zhang et al. (2011a) interpreted the Selin Co basin as a Gangdese retroarc foreland basin and include north-directed thrusts along the SNMZ as part of the retroarc thrust system (Fig. 14C), which is well-studied in the southern Lhasa terrane (Kapp et al., 2007b; Pullen et al., 2008a; He et al., 2007; Leier et al., 2007a). In this scenario, the GNT and the Duoni Formation would be components of the retroarc system. The provenance of the Takena Formation in the Linzhou basin, which represents the retroarc foreland basin fill, is primarily sourced from the Gangdese arc (Leier et al., 2007a). This is compatible with a paleoelevation study indicating the existence of an Andean-type mountain range (Gangdese) prior to the India-Asia collision (Ding et al., 2014).

However, these two interpretations are not compatible with the provenance results in this study. As discussed earlier, the provenance of the Cretaceous strata in Selin Co is primary the Cretaceous igneous rocks in the north part of the Lhasa terrane and the Paleozoic strata in Central Lhasa terrane (Fig. 13). Moreover, the timing of the retroarc thrust system and foreland thrusts along the BNSZ is later than c.a. 105 Ma (Kapp et al., 2003a, 2007a, 2007b; Volkmer et al., 2007; Pullen et al., 2008a; He et al., 2007; Leier et al., 2007a) (Fig. 13). Although the time of initiation of these faults cannot be constrained by the data in this study, we envision that the thrusts can be as early as the Early Cretaceous, earlier than the other two thrust systems (Fig. 13). As mentioned above, the Late Jurassic-Early Cretaceous Rila Formation shows indications of being affected by structural movement during deposition. To the west of the study area, Ding and Lai, 2003 reported the $Ar^{40}/Ar^{39}$ muscovite cooling age of c.a. 130 Ma for Wenbu granite in the hanging wall of the GNT. It is the oldest cooling age reported in the area along the east-west striking thrust belt and is interpreted as the time exhumation facilitated by the GNT initiated. The mean age of the youngest age cluster of the sample from the base of Early Cretaceous Eshaerbu Formation is also c.a. 130 Ma, which is interpreted as the age of deposition (Zhang Q. H. et al., 2011a). The ages of interbedded volcanic rocks in Early Cretaceous Duoni Formation are 112–125 Ma

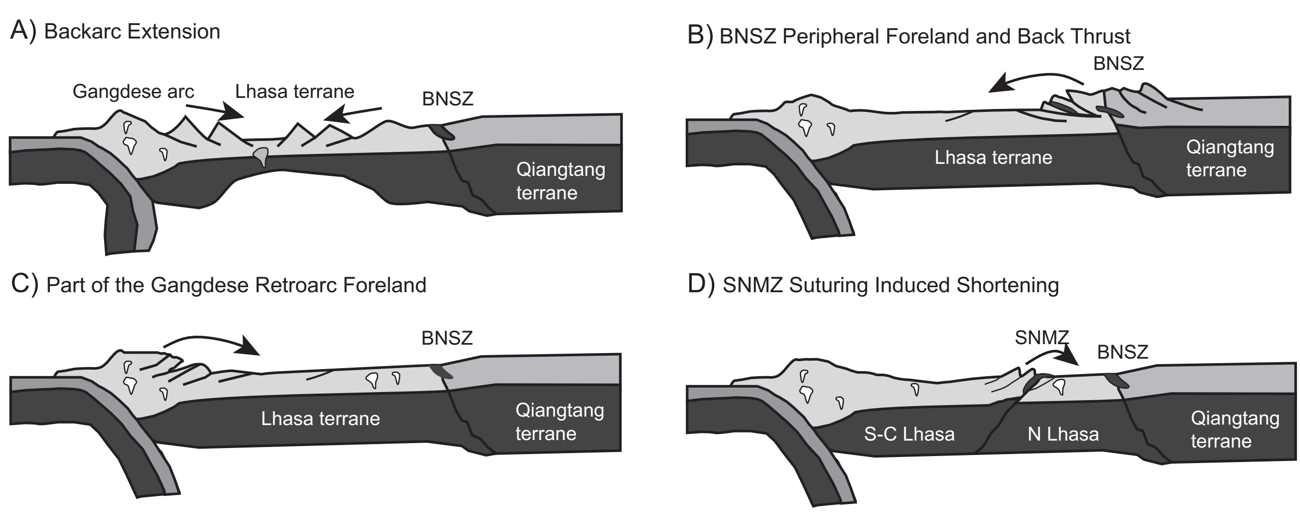


**Fig. 14.** Competing models accounting for crustal shortening and basin development in the north part of the Lhasa terrane in the Early Cretaceous. The black arrows stand for the erosion-to-deposition direction. A is back arc extensional basin model (e.g., Zhang et al., 2012). B indicates that the GNT could be a back thrust of the foreland thrust system in BNSZ (e.g., Murphy et al., 1997; Kapp et al., 2007a; Volkmer et al., 2007). C indicates that the GNT is part of the Gangdese retroarc thrust system (e.g., Zhang et al., 2011). D indicates that the GNT is a product of shortening along SNMZ, and is independent of and earlier than foreland thrusts along the BNSZ and Gangdese retroarc thrust system. D is the preferred model in this study.

(U-Pb zircon ages, Zhang Q. H. et al., 2011a and this study). Considering our interpretation of the provenance of these Early Cretaceous strata, and that the paleoflow direction of strata to the north of the GNT is primary to the north, it is reasonable to suggest that the initiation of thrusting and concomitant surface uplift can be as early as Late Jurassic-Early Cretaceous. Therefore, if the GNT is part of the retroarc thrust system it would be one of the earliest structures in its development and lie in the most foreland position of the thrust wedge. In this scenario, the SNMZ could have preferentially been reactivated during the earliest face of the retroarc shortening, due to earlier southward subduction (Fig. 14D). Regardless of the tectonic setting, development of the GNT facilitated the exhumation of the Paleozoic strata in the hangingwall of GNT and influenced sediment dispersal systems (Figs. 13 and 14D). In this model, the north-directed GNT, developed along a suture zone within the Lhasa terrane (SNMZ), in its initial stage, was an independent thrust from the BNSZ and the retroarc thrust system (Fig. 14D).

#### 7.4.3. Causes of early Cretaceous magmatism

The three volcanic rocks and three intrusive rocks yield Early Cretaceous ages of 105–120 Ma. In the Early Cretaceous, extensive magmatism occurred in an east-west belt at the northern part of the Lhasa terrane. The peak of these activities is at 110 Ma (Zhu et al., 2009). Geochemistry data of these rocks indicates that they were generated in a back-arc setting above a subduction zone (Hsü et al., 1995; Zhu et al., 2006, 2009; Kang et al., 2009; Ma and Yue, 2010; Qu et al., 2012; Sui et al., 2013; Chen et al., 2014; Wu et al., 2015). The igneous rocks analyzed in this study might have a similar origin.

Previously, researchers explained the magmatism in the north part of the Lhasa terrane to be due to southward subduction of Bangong-Nujiang oceanic lithosphere under the Lhasa terrane (e.g. Zhu et al., 2009; Qu et al., 2012; Chen et al., 2014) or by flat-subduction of Neo-Tethyan oceanic lithosphere northward under the Lhasa terrane (e.g. Coulon et al., 1986; Kapp et al., 2007a; Zhang et al., 2012). However, neither of the models can explain all the observations. While Zhu et al. (2009) proposed a model whereby the Bangong-Nujiang ocean was subducted southward based on the existence of igneous rocks in the Central and Northern Lhasa, the extensive Mesozoic igneous rocks in the southern part of the Qiangtang terrane (Li et al., 2014b; Liu et al., 2014; Fan et al., 2015; Li et al., 2015; Xu et al., 2015; Hao et al., 2016; Zeng et al., 2016) were considered by many researchers as evidence for northward subduction. Zhu et al. (2016) revised this model by incorporating divergent subduction zones to account for this problem. The Neo-Tethyan ocean flat-subduction model was originally proposed based on the absence of magmatism from c.a. 120 Ma to ca. 80 Ma in the Lhasa terrane (Coulon et al., 1986). However, since this model was proposed several Early Cretaceous igneous rocks with arc-lava signatures have been documented (Wen et al., 2008; Ji et al., 2009a, 2009b; Zhu et al., 2009 and references therein), which challenge the validity of this model.

Here we propose an alternative explanation for Early Cretaceous magmatism in the Northern and Central Lhasa. We envision that, in the suturing process along the SNMZ, subduction of an oceanic slab beneath the northern or central Lhasa terrane followed by slab rollback or wholesale delamination have induced the extensive magmatism during Early Cretaceous in the Central and Northern Lhasa terrane. This hypothesis predicts more convergence between the Lhasa terrane and the Southern Qiangtang terrane than models that correlated BNSZ ophiolites to SNMZ ophiolites.

## 8. Conclusion

Our study in the Xainza area provided new results bearing on several issues concerning the origin and tectonic evolution of the Lhasa terrane prior to the India-Asia collision. Specifically, the new constraints on the nature and evolution of the SNMZ revealed a more complicated Late Mesozoic geological history of the Lhasa terrain than previously thought, providing new perspectives on the magmatism, sedimentation, and structural evolution of the south Tibet.

Detrital zircon ages data from the Permian Angjie Formation shows affinity with Southern Qiangtang and the Himalayas, indicating that Lhasa terrane was once connected with the northern margin of the Indian subcontinent rather than Australia.

During the Triassic, less deposition occurred in the northern-central Lhasa terrane. Compared to the extensive Late Triassic deposits in the Qiangtang terrane and southern Lhasa terrane. One outstanding feature of Duoburi Formation in Xainza area is the lack of detrital zircons younger than 450 Ma. The distribution of ages younger than 450 Ma is similar to Carboniferous-Permian strata in the Central Lhasa terrane, which is interpreted as its provenance. There is not a significant amount of clastics from Qiangtang or south part of Lhasa contributing to the Duoburi Formation.

One gabbro sample from Yongzhu ophiolite yields a U-Pb zircon weighted mean age of 153.6 ± 2.3 Ma, indicating that the oceanic basin it represented formed in the Late Jurassic. The along strike difference in ages of SNMZ ophiolites may indicate opening of small ocean basins at different times along strike, possibly due to oblique rifting and subsequent seafloor spreading. Our results, combined with previously published results suggest that the SNMZ is a suture zone within the Lhasa terrane, separate from the BNSZ. The oceanic basin that Yongzhu ophiolite represents closed by the time of deposition of the Rila Formation in the Late Jurassic-Early Cretaceous.

North-directed thrust faults in Xainza area developed along the SNMZ. Slip along these thrusts juxtaposed the Paleozoic sequence and Yongzhu ophiolite to the south onto the Cretaceous basin to the north. The detrital zircon age data of Early Cretaceous Duoni Formation indicates that the source for these basin deposits is mainly the Jurassic-Cretaceous igneous rocks and Paleozoic strata to the south in Central Lhasa. The faults controlling this process could have initiated in the early Early Cretaceous, and driven by suturing of Northern and Central Lhasa subterranes.

Three volcanic rocks and three intrusive rocks from the study area yield ages of 105–120 Ma. All of them are intermediate-felsic rocks. The Northern Lhasa terrane experienced a period of extensive magmatism during Early Cretaceous, of which the peak was at c.a. 110 Ma. Previous studies suggested it was caused either by the rollback of northward plate-subduction of Neo-Tethys oceanic lithosphere or by the break-off or southward subduction of Bangong-Nujiang oceanic lithosphere. An alternative explanation presented here calls upon subduction and later delamination of oceanic lithosphere between the Northern and Central Lhasa.

## Acknowledgements

This study was financially supported by grants from the National Research and Development Plan [grant 2016YFC0600303]; the Chinese Academy of Sciences [grant XDB03010401]; and National Natural Science Foundation of China [grant 41490615]. We are thankful to Alexander Robinson, Jamey Jones, and an anonymous reviewer for their helpful reviews which greatly improved an earlier version of this manuscript.

## Appendix A. Supplementary data

Supplementary data to this article can be found online at https://doi.org/10.1016/j.tecto.2017.10.022.

## References

Aikman, A.B., Harrison, T.M., Lin, D., 2008. Evidence for early (> 44 Ma) Himalayan crustal thickening, Tethyan Himalaya, southeastern Tibet. Earth Planet. Sci. Lett. 274 (1–2), 14–23.

Aitchison, J.C., Xia, X., Baxter, A.T., Ali, J.R., 2011. Detrital zircon U–Pb ages along the Yarlung-Tsangpo suture zone, Tibet: implications for oblique convergence and collision between India and Asia. Gondwana Res. 20 (4), 691–709.
Allégre, C.O., Courtillot, V., Tapponnier, P., Hirn, A., Mattauer, M., Coulon, C., Jaeger, J., Achache, J., Schärer, U., Marcoux, J., 1984. Structure and Evolution of the Himalaya–Tibet Orogenic Belt.
Baxter, A.T., Aitchison, J.C., Zyabrev, S.V., 2009. Radiolarian age constraints on Mesotethyan ocean evolution, and their implications for development of the Bangong-Nujiang suture, Tibet. J. Geol. Soc. 166 (4), 689–694.
BGMRXAR (Bureau of Geology Mineral Resources of Xizang Autonomous Region), 1993. Regional Geology of Xizang (Tibet) Autonomous Region. Geological Publishing House, Beijing, pp. 1–450 (in Chinese with English abstract).
Bird, P., 1978. Initiation of intracontinental subduction in the Himalaya. J. Geophys. Res. Solid Earth 83 (B10), 4975–4987.
Cai, F., Ding, L., Leary, R.J., Wang, H., Xu, Q., Zhang, L., Yue, Y., 2012. Tectonostratigraphy and provenance of an accretionary complex within the Yarlung–Zangpo suture zone, southern Tibet: insights into subduction–accretion processes in the Neo-Tethys. Tectonophysics 574–575, 181–192.
Cai, F., Ding, L., Laskowski, A.K., Kapp, P., Wang, H., Xu, Q., Zhang, L., 2016. Late Triassic paleogeographic reconstruction along the Neo–Tethyan Ocean margins, southern Tibet. Earth Planet. Sci. Lett. 435, 105–114.
Cawood, P.A., Nemchin, A.A., 2000. Provenance record of a rift basin: U/Pb ages of detrital zircons from the Perth Basin, Western Australia. Sediment. Geol. 134 (3–4), 209–234.
Chemenda, A.I., Burg, J.-P., Mattauer, M., 2000. Evolutionary model of the Himalaya–Tibet system: geopoem: based on new modelling, geological and geophysical data. Earth Planet. Sci. Lett. 174 (3), 397–409.
Chen, S.Y., Yang, J.S., Li, Y., Xu, X.Z., 2009. Ultramafic blocks in Sumdo region, Lhasa block Eastern Tibet plateau: an ophiolite unit. J. Earth Sci. 20 (2), 332–347.
Chen, Y., Zhu, D.C., Zhao, Z.D., Meng, F.Y., Wang, Q., Santosh, M., Wang, L.Q., Dong, G.C., Mo, X.X., 2014. Slab breakoff triggered ca. 113 Ma magmatism around Xainza area of the Lhasa Terrane, Tibet. Gondwana Res. 26 (2), 449–463.
Chu, M.F., Chung, S.L., Song, B., Liu, D., O'Reilly, S.Y., Pearson, N.J., Ji, J., Wen, D.J., 2006. Zircon U-Pb and Hf isotope constraints on the Mesozoic tectonics and crustal evolution of southern Tibet. Geology 34 (9), 745–748.
Coulon, C., Maluski, H., Bollinger, C., Wang, S., 1986. Mesozoic and cenozoic volcanic rocks from central and southern Tibet: 39Ar-40Ar dating, petrological characteristics and geodynamical significance. Earth Planet. Sci. Lett. 79 (3), 281–302.
Coward, M., Kidd, W., Yun, P., et al., 1988. The structure of the 1985 Tibet geotraverse, Lhasa to Golmud. In: Philosophical Transactions of the Royal Society of London. Series A, Mathematical and Physical Sciences Vol 327. pp. 307–333 (no. 1594).
DeCelles, P.G., Kapp, P., Ding, L., Gehrels, G.E., 2007. Late Cretaceous to middle Tertiary basin evolution in the central Tibetan Plateau: changing environments in response to tectonic partitioning, aridification, and regional elevation gain. Geol. Soc. Am. Bull. 119 (5–6), 654–680.
Dewey, J.F., Shackleton, R.M., Chang, C.F., et al., 1988. The tectonic evolution of the Tibetan plateau. In: Philosophical Transactions of the Royal Society A. Mathematical, Physical and Engineering Sciences Vol 327. pp. 379–413 (no. 1594).
Dickinson, W.R., Suczek, C.A., 1979. Plate tectonics and sandstone compositions. AAPG Bull. 63 (12), 2164–2182.
Ding, L., Lai, Q.Z., 2003. New geological evidence of crustal thickening in the Gangdese block prior to the Indo-Asian collision. Chin. Sci. Bull. 48 (15), 1604–1610.
Ding, L., Yang, D., Cai, F.L., Pullen, A., Kapp, P., Gehrels, G.E., Zhang, L.Y., Zhang, Q.H., Lai, Q.Z., Yue, Y.H., Shi, R.D., 2013. Provenance analysis of the Mesozoic Hoh-Xil-Songpan-Ganzi turbidites in northern Tibet: implications for the tectonic evolution of the eastern Paleo-Tethys Ocean. Tectonics 32, 34–48.
Ding, L., Xu, Q., Yue, Y.H., Wang, H.Q., Cai, F.L., Li, S., 2014. The Andean-type Gangdese Mountains: Paleoelevation record from the Paleocene–Eocene Linzhou Basin. Earth Planet. Sci. Lett. 392, 250–264.
Dong, Y.H., Xu, J.F., Zeng, Q.G., Wang, Q., Mao, G.Z., Li, J., 2006. Is there a Neo-Tethys' subduction record earlier than arc volcanic rocks in the Sangri Group? Acta Petrol. Sin. 22 (3), 661–668 (in Chinese with English abstract).
Dong, X., Zhang, Z., Liu, F., Wang, W., Yu, F., Shen, K., 2011. Zircon U–Pb geochronology of the Nyainqentanglha Group from the Lhasa terrane: new constraints on the Triassic orogeny of the south Tibet. J. Asia Earth Sci. 42 (4), 732–739.
Eyles, Eyles, 2000. Subaqueous mass flow origin for Lower Permian diamictites and associated facies of the Grant Group, Barbwire Terrace, Canning Basin, Western Australia. Sedimentology 47 (2), 343–356.
Eyles, N., Mory, A.J., Eyles, C.H., 2006. 50-million-year-long record of glacial to post-glacial marine environments preserved in a carboniferous–Lower Permian Graben, Northern Perth Basin, Western Australia. J. Sediment. Res. 76 (3), 618–632.
Fan, S.Q., Shi, R.D., Ding, L., Liu, D.L., Huang, Q.S., Wang, H.Q., 2010. Geochemical characteristics and zircon U-Pb age of the plagiogranite in Gaize ophiolite of central Tibet and their tectonic significance. Acta Petrol. Mineral. 29 (5), 467–478 (in Chinese with English abstract).
Fan, J.J., Li, C., Liu, Y.M., Xu, J.X., 2015. Age and nature of the late Early Cretaceous Zhaga Formation, northern Tibet: constraints on when the Bangong–Nujiang Neo-Tethys Ocean closed. Int. Geol. Rev. 57 (3), 342–353.
Fu, X.G., Wang, J., Tan, F.W., Chen, M., Chen, W.B., 2010. The Late Triassic rift-related volcanic rocks from eastern Qiangtang, northern Tibet (China): Age and tectonic implications. Gondwana Res. 17 (1), 135–144.
Fu, J.J., Ding, L., Xu, Q., Cai, F.L., Yue, Y.H., Guo, Y., 2015. Zircon U-Pb geochronology and Hf isotopic composition of the cretaceous volcanic rocks and constraint of the collision age of Bangong-Nujiang suture zone in Dongco area, Gaize, Tibet. Chin. J. Geol. 50 (1), 182–202 (in Chinese with English abstract).
Gao, S.B., Zheng, Y.Y., Wang, J.S., Zhang, Z., Yang, C., 2011. The geochronology and geochemistry of intrusive rocks in Bange area: constraints on the evolution time of the Bangong Lake-Nujiang ocean basin. Acta Petrol. Sin. 27 (7), 1973–1982 (in Chinese with English abstract).
Gehrels, G., Kapp, P., DeCelles, P., et al., 2011. Detrital zircon geochronology of pre-Tertiary strata in the Tibetan-Himalayan orogen. Tectonics 30 (TC5016). http://dx.doi.org/10.1029/2011TC002868.
Geng, Q.R., Pan, G.T., Wang, L.Q., Zhu, D.C., Liao, Z.L., 2006. Isotopic geochronology of the volcanic rocks from the Yeba Formation in the Gangdise zone, Xizang. Sediment. Geol. Tethyan Geol. 26 (1), 1–7 (in Chinese with English abstract).
Geng, Q.R., Pan, G.T., Wang, L.Q., Peng, Z.M., Zhang, Z., 2011. Tethyan evolution and metallogenic geological background of the Bangong Co-Nujiang belt and the Qiangtang massif in Tibet. Geol. Bull. China 30 (8), 1261–1274 (in Chinese with English abstract).
Girardeau, J., Marcoux, J., Allegre, C., et al., 1984. Tectonic environment and geodynamic significance of the Neo-Cimmerian Donqiao ophiolite, Bangong-Nujiang suture zone, Tibet. Nature 307, 27–31.
Girardeau, J., Marcoux, J., Fourcade, E., et al., 1985. Xainxa ultramafic rocks, central Tibet, China: tectonic environment and geodynamic significance. Geology 13 (5), 330–333.
Guo, L., Liu, Y., Liu, S., Cawood, P.A., Wang, Z., Liu, H., 2013. Petrogenesis of early to middle Jurassic granitoid rocks from the Gangdese belt Southern Tibet: implications for early history of the Neo-Tethys. Lithos 179, 320–333.
Hao, L.L., Wang, Q., Wyman, D.A., Ou, Q., Dan, W., Jiang, Z.Q., Yang, J.H., Li, J., Long, X.P., 2016. Andesitic crustal growth via mélange partial melting: evidence from Early Cretaceous arc dioritic/andesitic rocks in southern Qiangtang, central Tibet. Geochem. Geophys. Geosyst. 17 (5), 1641–1659.
He, Z.H., Yang, D.M., Zheng, C.Q., Wang, T.W., 2006a. Isotopic dating of the Mamba granitoid in the Gangdise tectonic belt and its constraint on the subduction time of the Neotethys. Geol. Rev. 52 (1), 100–106 (in Chinese with English abstract).
He, Z.H., Yang, D.M., Wang, T.W., 2006b. Age, geochemistry and its tectonic significance of Kaimeng ophiolites in Jiali fault belt, Tibet. Acta Petrol. Sin. 22 (3), 653–660 (in Chinese with English abstract).
He, S.D., Kapp, P., DeCelles, P.G., Gehrels, G.E., Heizler, M., 2007. Cretaceous–Tertiary geology of the Gangdese Arc in the Linzhou area, southern Tibet. Tectonophysics 433 (1–4), 15–37.
Hsü, K.J., Guitang, P., Sengör, A.M.C., 1995. Tectonic evolution of the Tibetan Plateau: a working hypothesis based on the archipelago model of orogenesis. Int. Geol. Rev. 37 (6), 473–508.
Ingersoll, R.V., Suczek, C.A., 1979. Petrology and provenance of Neogene sand from Nicobar and Bengal fans, DSDP sites 211 and 218. J. Sediment. Res. 49 (4), 1217–1228.
Ingersoll, R.V., Fullard, T.F., Ford, R.L., Grimm, J.P., Pickle, J.D., Sares, S.W., 1984. The effect of grain size on detrital modes; a test of the Gazzi-Dickinson point-counting method. J. Sediment. Res. 54 (1), 103–116.
Ji, W.H., Chen, S.J., Zhao, Z.M., Li, R.S., He, S.P., Wang, C.D., 2009a. Discovery of the Cambiran volcanic rocks in the Xainza area, Gangdese orogenic belt, Tibet, China and its significance. Geol. Bull. Chin. 28 (9), 1350–1354 (in Chinese with English abstract).
Ji, W.Q., Wu, F.Y., Chung, S.L., Li, J.X., Liu, C.Z., 2009b. Zircon U–Pb geochronology and Hf isotopic constraints on petrogenesis of the Gangdese batholith, southern Tibet. Chem. Geol. 262 (3–4), 229–245.
Jin, X., 2002. Permo-Carboniferous sequences of Gondwana affinity in southwest China and their paleogeographic implications. J. Asian Earth Sci. 20 (6), 633–646.
Kang, Z.Q., Xu, J.F., Wang, B.D., Dong, Y.H., Wang, S.Q., Chen, J.L., 2009. Geochemistry of Cretaceous volcanic rocks of Duoni Formation in northern Lhasa block: discussion of tectonic setting. Earth Sci. J. China Univ. Geosci. 34, 89–104 (in Chinese with English abstract).
Kang, Z.Q., Xu, J.F., Wilde, S.A., Feng, Z.H., Chen, J.L., Wang, B.D., Fu, W.C., Pan, H.B., 2014. Geochronology and geochemistry of the Sangri Group Volcanic Rocks, Southern Lhasa Terrane: implications for the early subduction history of the Neo-Tethys and Gangdese Magmatic Arc. Lithos 200–201, 157–168.
Kapp, J.L.D., Harrison, T.M., Kapp, P., Grove, M., Lovera, O.M., Ding, L., 2005. Nyainqentanglha Shan: a window into the tectonic, thermal, and geochemical evolution of the Lhasa block, southern Tibet. J. Geophys. Res. 110 (B08413). http://dx.doi.org/10.1029/2004JB003330.
Kapp, P., Yin, A., Manning, C.E., Murphy, M., Harrison, T.M., Spurlin, M., Lin, D., Xi-Guang, D., Cun-Ming, W., 2000. Blueschist-bearing metamorphic core complexes in the Qiangtang block reveal deep crustal structure of northern Tibet. Geology 28 (1), 19.
Kapp, P., Murphy, M.A., Yin, A., et al., 2003a. Mesozoic and Cenozoic tectonic evolution of the Shiquanhe area of western Tibet. Tectonics 22, 1029. http://dx.doi.org/10.1029/2001TC001332.
Kapp, P., Yin, A., Manning, C.E., Harrison, T.M., Taylor, M.H., Ding, L., 2003b. Tectonic evolution of the early Mesozoic blueschist-bearing Qiangtang metamorphic belt, central Tibet. Tectonics 22 (4). http://dx.doi.org/10.1029/2002tc001383.
Kapp, P., DeCelles, P.G., Gehrels, G.E., Heizler, M., Ding, L., 2007a. Geological records of the Lhasa-Qiangtang and Indo-Asian collisions in the Nima area of central Tibet. Geol. Soc. Am. Bull. 119 (7–8), 917–933.
Kapp, P., DeCelles, P.G., Leier, A.L., Fabijanic, J.M., He, S., Pullen, A., Gehrels, G.E., Ding, L., 2007b. The Gangdese retroarc thrust belt revealed. GSA Today 17 (7), 4.
Leeder, M.R., Smith, A.B., Jixiang, Y., 1988. Sedimentology, palaeoecology and palaeoenvironmental evolution of the 1985 Lhasa to Golmud Geotraverse. In: Philosophical Transactions of the Royal Society A. Mathematical, Physical and Engineering Sciences Vol 327. pp. 107–143 (no. 1594).
Leier, A.L., DeCelles, P.G., Kapp, P., Ding, L., 2007a. The Takena Formation of the Lhasa terrane, southern Tibet: the record of a Late Cretaceous retroarc foreland basin. Geol.

Soc. Am. Bull. 119 (1–2), 31–48.
Leier, A.L., DeCelles, P.G., Kapp, P., Gehrels, G.E., 2007b. Lower Cretaceous strata in the Lhasa terrane Tibet, with implications for understanding the early tectonic history of the Tibetan Plateau. J. Sediment. Res. 77 (10), 809–825.
Leier, A.L., Kapp, P., Gehrels, G.E., DeCelles, P.G., 2007c. Detrital zircon geochronology of Carboniferous - Cretaceous strata in the Lhasa terrane Southern Tibet. Basin Res. 19 (3), 361–378.
Li, C., Wang, T.W., Li, H.M., Zeng, Q.G., 2003. Discovery of Indosinian megaporphyritic granodiorite in the Gangdise area: evidence for the existence of Paleo-Gangdise. Geol. Bull. Chin. 22 (5), 364–366 (in Chinese with English abstract).
Li, H.Q., Cai, Z.H., Chen, S.Y., Tang, Z.M., Yang, M., 2008. The Indosinian Orogenesis Occurred in Lhasa Terrain and the Evidence from Muscovite 40Ar-39Ar Geochronology. Vol 24 (no. 7). pp. 1595–1604.
Li, C., Zhai, Q.G., Dong, Y.S., Liu, S., Xie, C.M., Wu, Y.W., 2009. High-pressure eclogite-blueschist metamorphic belt and closure of paleo-Tethys Ocean in Central Qiangtang, Qinghai-Tibet plateau. J. Earth Sci. 20 (2), 209–218.
Li, G.W., Liu, X.H., Alex, P., Wei, L.J., Liu, X.B., Huang, F.X., Zhou, X.J., 2010. In-situ detrital zircon geochronology and Hf isotopic analyses from Upper Triassic Tethys sequence strata. Earth Planet. Sci. Lett. 297 (3–4), 461–470.
Li, H.Q., Xu, Z.Q., Yang, J.S., Tang, Z.M., Yang, M., 2011. Syn-collisional exhumation of Sumdo eclogite in the Lhasa Terrane, Tibet: evidences from structural deformation and $^{40}Ar$-$^{39}Ar$ geochronology. Earth Sci. Front. 18 (3), 066–078 (in Chinese with English abstract).
Li, G.W., Sandiford, M., Liu, X.H., Xu, Z.Q., Wei, L.J., Li, H.Q., 2014a. Provenance of Late Triassic sediments in central Lhasa terrane, Tibet and its implication. Gondwana Res. 25 (4), 1680–1689.
Li, S.M., Zhu, D.C., Wang, Q., Zhao, Z.D., Sui, Q.L., Liu, S.A., Liu, D., Mo, X.X., 2014b. Northward subduction of Bangong–Nujiang Tethys insight from Late Jurassic intrusive rocks from Bangong Tso in western Tibet. Lithos 205, 284–297.
Li, Y., He, J., Wang, C., Han, Z., Ma, P., Xu, M., Du, K., 2015. Cretaceous volcanic rocks in south Qiangtang Terrane: products of northward subduction of the Bangong–Nujiang Ocean? J. Asian Earth Sci. 104, 69–83.
Li, S., Ding, L., Guilmette, C., Fu, J., Xu, Q., Yue, Y., Henrique-Pinto, R., 2017. The subduction-accretion history of the Bangong-Nujiang Ocean: constraints from provenance and geochronology of the Mesozoic strata near Gaize, central Tibet. Tectonophysics 702, 42–60.
Liang, X., Wang, G., Yuan, G., Liu, Y., 2012. Structural sequence and geochronology of the Qomo Ri accretionary complex, Central Qiangtang, Tibet: implications for the Late Triassic subduction of the Paleo-Tethys Ocean. Gondwana Res. 22 (2), 470–481.
Liu, Q.S., Jiang, W., Jian, P., Ye, P.S., Wu, Z.H., Hu, D.G., 2006. Zircon SHRIMP U-Pb age and petrochemical and geochemical features of Mesozoic muscovite monzonitic granite at Ningzhong, Tibet. Acta Petrol. Sin. 22 (3), 643–652 (in Chinese with English abstract).
Liu, D.L., Huang, Q.S., Fan, S.Q., Zhang, L.Y., Shi, R.D., Ding, L., 2014. Subduction of the Bangong-Nujiang Ocean: constraints from granites in the Bangong Co area, Tibet. Geol. J. 49 (2), 188–206.
Ludwig, K.R., 2003. User's Manual for Isoplot 3.00: A Geochronological Toolkit for Microsoft Excel. Berkeley Geochronology Center Special Publication, California, pp. 1–700.
Ma, G.L., Yue, Y.H., 2010. Cretaceous volcanic rocks in northern Lhasa Block: constraints on the tectonic evolution of the Gangdese Arc. Acta Petrol. Mineral. 29, 525–538 (in Chinese with English abstract).
Meng, Y., Xu, Z., Santosh, M., Ma, X., Chen, X., Guo, G., Liu, F., 2015. Late Triassic crustal growth in southern Tibet: evidence from the Gangdese magmatic belt. Gondwana Res. 37, 449–464.
Metcalfe, I., 1996. Gondwanaland dispersion, Asian accretion and evolution of eastern Tethys∗. Aust. J. Earth Sci. 43 (6), 605–623.
Metcalfe, I., 2009. Late Palaeozoic and Mesozoic tectonic and palaeogeographical evolution of SE Asia. Geol. Soc. Lond. Spec. Publ. 315 (1), 7–23.
Murphy, M., Yin, A., Harrison, T., Dürr, S., Chen, Z., Ryerson, F., Kidd, W., Wang, X., Zhou, X., 1997. Did the Indo-Asian collision alone create the Tibetan plateau? Geology 25 (8), 719–722.
Pan, G.T., Ding, J., Yao, D.S., et al., 2004. Guidebook of 1:1,500,000 Geologic Map of the Qinghai–Xizang (Tibet) Plateau and Adjacent Areas. Cartographic Publishing House, Chengdu, China, pp. 1–148.
Pan, G.T., Mo, X.X., Hou, Z.Q., et al., 2006. Spatial–temporal framework of the Gangdese Orogenic Belt and its evolution. Acta Petrol. Sin. 22, 521–533 (in Chinese with English abstract).
Pan, G.T., Wang, L., Li, R., et al., 2012. Tectonic evolution of the Qinghai-Tibet Plateau. J. Asian Earth Sci. 53, 3–14.
Pearce, J.A., Deng, W., 1988. The ophiolites of the Tibetan Geotraverses, Lhasa to Golmud (1985) and Lhasa to Kathmandu (1986). In: Philosophical Transactions of the Royal Society of London. Series A, Mathematical and Physical Sciences Vol 327. pp. 215–238.
Pearce, J.A., Mei, H., 1988. Volcanic rocks of the 1985 Tibet Geotraverse: Lhasa to Golmud. In: Philosophical Transactions of the Royal Society A. Mathematical, Physical and Engineering Sciences Vol 327 (no. 1594). pp. 169–201.
Press, W.H., Flannery, B.P., Teukolsky, S.A., Vetterling, W.T., 1986. Numerical Recipes: The Art of Scientific Computing. Cambridge, MA, Cambridge U Press.
Pullen, A., Kapp, P., Gehrels, G.E., DeCelles, P.G., Brown, E.H., Fabijanic, J.M., Ding, L., 2008a. Gangdese retroarc thrust belt and foreland basin deposits in the Damxung area, southern Tibet. J. Asian Earth Sci. 33 (5–6), 323–336.
Pullen, A., Kapp, P., Gehrels, G.E., Vervoort, J.D., Ding, L., 2008b. Triassic continental subduction in central Tibet and Mediterranean-style closure of the Paleo-Tethys Ocean. Geology 36 (5), 351.
Pullen, A., Kapp, P., Gehrels, G.E., Ding, L., Zhang, Q., 2011. Metamorphic rocks in central Tibet: lateral variations and implications for crustal structure. Geol. Soc. Am. Bull. 123 (3–4), 585–600.
Qiu, R.Z., Zhou, S., Li, T.D., Deng, J.F., Xiao, Q.H., Wu, Z.X., Cai, Z.Y., 2007. The tectonic-setting of ophiolites in the western Qinghai-Tibet Plateau, China. J. Asian Earth Sci. 29 (2–3), 215–228.
Qu, Y.G., Wang, Y.S., Zhang, S.Q., Lu, P., Jiang, X.F., 2003a. An inspiration from the section of the Late Triassic Duoburi Formation in the Xainza area-Stratigraphic constraints on the Indosinian movement in Gangdise. Geol. Bull. Chin. 22, 470–473 (in Chinese with English abstract).
Qu, Y.G., Zhang, S.Q., Zheng, C.Z., Wang, Y.S., Lv, P., Wang, H.S., Li, X.B., Li, X.W., 2003b. The Late Jurassic-Early Cretaceous Rila Formation, Rila Formation Suor clastic rocks and Characteristics of biotas in the Yunzhug ophiolite belt, northern Tibet. Geol. Bull. Chin. 22 (11–12), 959–963 (in Chinese with English abstract).
Qu, Y.G., Wang, Y.S., Duan, J.X., 2011. 1:250, 000 Geological Report of Duoba with Geological Map. Institute of Geological Survey, Jilin University, Changchun (in Chinese).
Qu, X.M., Wang, R.J., Xin, H.B., Jiang, J.H., Chen, H., 2012. Age and petrogenesis of A-type granites in the middle segment of the Bangonghu–Nujiang suture, Tibetan plateau. Lithos 146-147, 264–275.
Saylor, J.E., Jordan, J.C., Sundell, K.E., Wang, X., Wang, S., Deng, T., 2017. Topographic growth of the Jishi Shan and its impact on basin and hydrology evolution NE Tibetan Plateau. Basin Res. http://dx.doi.org/10.1111/bre.12264. (Accepted Author Manuscript).
Shi, R., Yang, J., Xu, Z., Qi, X., 2004. Discovery of the boninite series volcanic rocks in the Bangong Lake ophiolite melange, western Tibet, and its tectonic implications. Chin. Sci. Bull. 49 (12), 1272–1278.
Song, S.W., Liu, Z., Zhu, D.C., Wang, Q., Zhang, L.Z., Zhang, L.L., Zhao, Z.D., 2014. Zircon U-Pb chronology and Hf isotope of the late Triassic andesitic magmatism in Dajiacuo. Tibet. Acta Petrol. Sin. 30 (10), 3100–3112.
Sui, Q.L., Wang, Q., Zhu, D.C., Zhao, Z.D., Chen, Y., Santosh, M., Hu, Z.C., Yuan, H.L., Mo, X.X., 2013. Compositional diversity of ca. 110 Ma magmatism in the northern Lhasa Terrane, Tibet: implications for the magmatic origin and crustal growth in a continent–continent collision zone. Lithos 168–169, 144–159.
Tang, F.L., Huang, J.C., Luo, X.C., Huang, C.G., 2004. The discovery and significance of the Asuo structural mélange in North Tibet. J. East Chin. Inst. Technol. 27, 245–250 (in Chinese with English abstract).
Tapponnier, P., Zhiqin, X., Roger, F., Meyer, B., Arnaud, N., Wittlinger, G., Jingsui, Y., 2001. Oblique stepwise rise and growth of the Tibet Plateau. Science 294, 1671–1677.
Veevers, J.J., Saeed, A., Belousova, E.A., Griffin, W.L., 2005. U–Pb ages and source composition by Hf-isotope and trace-element analysis of detrital zircons in Permian sandstone and modern sand from southwestern Australia and a review of the paleogeographical and denudational history of the Yilgarn Craton. Earth Sci. Rev. 68 (3–4), 245–279.
Vermeesch, P., 2013. Multi-sample comparison of detrital age distributions. Chem. Geol. 341, 140–146.
Volkmer, J.E., Kapp, P., Guynn, J.H., Lai, Q., 2007. Cretaceous-tertiary structural evolution of the north central Lhasa terrane, Tibet. Tectonics 26 (TC6007). http://dx.doi.org/10.1029/2005TC001832.
Volkmer, J.E., Kapp, P., Horton, B.K., Gehrels, G.E., Minervini, J.M., Ding, L., 2014. Northern Lhasa thrust belt of central Tibet: evidence of Cretaceous–early Cenozoic shortening within a passive roof thrust system? Geol. Soc. Am. Spec. Pap. 507, 59–70.
Wang, Y.S., Qu, Y.G., Lv, P., Wang, Z.H., Zhang, S.Q., 2003. The geologic features of ophiolite zone in the Yongzhu area, Tibet. Jilin Geology 22, 1–14 (in Chinese with English abstract).
Wang, B.D., Xu, J.F., Zeng, Q.G., Kang, Z.Q., Chen, J.L., Dong, Y.H., 2007. Geochemistry and genesis of Lhaguo Tso ophiolite in south of Gerze area, Center Tibet. Acta Petrol. Sin. 23 (6), 1521–1530 (in Chinese with English abstract).
Wang, B.D., Wang, L.Q., Chung, S.L., Chen, J.L., Yin, F.G., Liu, H., Li, X.B., Chen, L.K., 2016a. Evolution of the Bangong–Nujiang Tethyan ocean: insights from the geochronology and geochemistry of mafic rocks within ophiolites. Lithos 245, 18–33.
Wang, C., Ding, L., Zhang, L.Y., Kapp, P., Pullen, A., Yue, Y.H., 2016b. Petrogenesis of Middle–Late Triassic volcanic rocks from the Gangdese belt, southern Lhasa terrane: implications for early subduction of Neo-Tethyan oceanic lithosphere. Lithos 262, 320–333.
Wang, C., Ding, L., Liu, Z.C., Zhang, L.Y., Yue, Y.H., 2017. Early Cretaceous bimodal volcanic rocks in the southern Lhasa terrane, south Tibet: age, petrogenesis and tectonic implications. Lithos 268–271, 260–273.
Webb, A.A.G., Yin, A., Harrison, T.M., Célérier, J., Gehrels, G.E., Manning, C.E., Grove, M., 2011. Cenozoic tectonic history of the Himachal Himalaya (northwestern India) and its constraints on the formation mechanism of the Himalayan orogen. Geosphere 7 (4), 1013–1061.
Webb, A.A.G., Yin, A., Dubey, C.S., 2013. U-Pb zircon geochronology of major lithologic units in the eastern Himalaya: implications for the origin and assembly of Himalayan rocks. GSA Bull. 125 (3–4), 499–522.
Wen, D., Liu, D., Chung, S., Chu, M., Ji, J., Zhang, Q., Song, B., Lee, T., Yeh, M., Lo, C., 2008. Zircon SHRIMP U–Pb ages of the Gangdese Batholith and implications for Neotethyan subduction in southern Tibet. Chem. Geol. 252 (3–4), 191–201.
Wu, F.Y., Ji, W.Q., Liu, C.Z., Chung, S.L., 2010. Detrital zircon U–Pb and Hf isotopic data from the Xigaze fore-arc basin: constraints on Transhimalayan magmatic evolution in southern Tibet. Chem. Geol. 271 (1–2), 13–25.
Wu, H., Li, C., Xu, M., Li, X., 2015. Early Cretaceous adakitic magmatism in the Dachagou area, northern Lhasa terrane Tibet: implications for slab roll-back and subsequent slab break-off of the lithosphere of the Bangong–Nujiang Ocean. J. Asian Earth Sci. 97, 51–66.
Xu, M., Li, C., Xu, W., et al., 2014. Petrology, geochemistry and geochronology of gabbros

from the Zhongcang ophiolitic mélange, central Tibet: implications for an intra-oceanic subduction zone within the Neo-Tethys Ocean. J. Earth Sci. 25 (2), 224–240.
Xu, W., Li, C., Xu, M.J., Wu, Y.W., Fan, J.J., Wu, H., 2015. Petrology, geochemistry, and geochronology of boninitic dikes from the Kangqiong ophiolite: implications for the Early Cretaceous evolution of Bangong–Nujiang Neo-Tethys Ocean in Tibet. Int. Geol. Rev. 57 (16), 2028–2043.
Yang, J.S., Xu, Z.Q., Li, Z.L., Xu, X.Z., Li, T.F., Ren, Y.F., Li, H.Q., Chen, S.Y., Robinson, P.T., 2009. Discovery of an eclogite belt in the Lhasa block, Tibet: a new border for Paleo-Tethys? J. Asian Earth Sci. 34 (1), 76–89.
Ye, P.S., Wu, Z.H., Hu, D.G., Jiang, W., Yang, X.D., 2004. Geochemistry and tectonic setting of ophiolites in west of Namco Lake, Tibet. Geoscience 18, 237–243 (in Chinese with English abstract).
Yin, A., Harrison, T.M., 2000. Geologic evolution of the Himalayan-Tibetan orogen. Annu. Rev. Earth Planet. Sci. 28 (1), 211–280.
Yin, A., Nie, S., 1993. An indentation model for the North and South China collision and the development of the Tan-Lu and Honam Fault Systems, eastern Asia. Tectonics 12 (4), 801–813.
Yin, J., Xu, J., Liu, C., Li, H., 1988. The Tibetan plateau: regional stratigraphic context and previous work. In: Philosophical Transactions of the Royal Society A. Mathematical, Physical and Engineering Sciences Vol 327. pp. 5–52 (no. 1594).
Yin, A., Harrison, T.M., Murphy, M., Grove, M., Nie, S., Ryerson, F., Feng, W.X., Le, C.Z., 1999. Tertiary deformation history of southeastern and southwestern Tibet during the Indo-Asian collision. Geol. Soc. Am. Bull. 111, 1644–1664.
Zeng, M., Zhang, X., Cao, H., Ettensohn, F.R., Cheng, W., Lang, X., 2016. Late Triassic initial subduction of the Bangong-Nujiang Ocean beneath Qiangtang revealed: stratigraphic and geochronological evidence from Gaize, Tibet. Basin Res. 28 (1), 147–157.
Zhai, Q.G., Jahn, B.M., Su, L., Wang, J., Mo, X.X., Lee, H.Y., Wang, K.L., Tang, S., 2013. Triassic arc magmatism in the Qiangtang area, northern Tibet: zircon U–Pb ages, geochemical and Sr–Nd–Hf isotopic characteristics, and tectonic implications. J. Asian Earth Sci. 63, 162–178.
Zhang, Y.X., Zhang, K.J., Li, B., Wang, Y., Wei, Q.G., Tang, X.C., 2007a. Zircon SHRIMP U-Pb geochronology and petrogenesis of the plagiogranites from the Lagkor Lake ophiolite, Gerze, Tibet, China. Chin. Sci. Bull. 52 (5), 651–659.
Zhang, H.F., Xu, W.C., Guo, J.Q., Zong, K.Q., Cai, H.M., Yuan, H.L., 2007b. Indosinian orogenesis of the Gangdese terrane: evidences from zircon U–Pb dating and petrogenesis of granitoids. Earth Sci J. China Univ. Geosci 32 (in Chinese with English abstract), 155–166.
Zhang, Q.H., Ding, L., Cai, F.L., Xu, X.X., Zhang, L.Y., Xu, Q., Willems, H., 2011a. Early Cretaceous Gangdese retroarc foreland basin evolution in the Selin Co basin, central Tibet: evidence from sedimentology and detrital zircon geochronology. Geol. Soc. Lond., Spec. Publ. 353 (1), 27–44.
Zhang, R., Murphy, M.A., Lapen, T.J., Sanchez, V., Heizler, M., 2011b. Late Eocene crustal thickening followed by Early-Late Oligocene extension along the India-Asia suture zone: evidence for cyclicity in the Himalayan orogen. Geosphere 7, 1249–1268.
Zhang, K.J., Zhang, Y.X., Tang, X.C., Xia, B., 2012. Late Mesozoic tectonic evolution and growth of the Tibetan plateau prior to the Indo-Asian collision. Earth-Sci. Rev. 114 (3–4), 236–249.
Zheng, L.L., Geng, Q.R., Dong, H., 2003. The discovery and significance of the relicts of ophiolitic mélanges along the Parlung Zangbo in the Bomi region, eastern Xizang. Sediment. Geol. Tethyan Geol. 23, 27–30 (in Chinese with English abstract).
Zheng, Y.Y., Xu, R.K., Ma, G.T., Gao, S.B., Zhang, G.Y., Ma, X.M., Ci, Q., 2006. Ages of generation and subduction of Shiquan river ophiolite: restriction from SHRIMP zircon dating. Acta Petrol. Sin. 22 (4), 895–904 (in Chinese with English abstract).
Zhong, Y., Xia, B., Liu, W.L., Yin, Z.X., Hu, X.C., Huang, W., 2015. Geochronology, petrogenesis and tectonic implications of the Jurassic Namco–Renco ophiolites, Tibet. Int. Geol. Rev. 57 (4), 508–528.
Zhu, Z., 2004. The Geochemical Characteristics and Tectonic Setting about Ophiolite in Yongzhu–Namucuo, Tibet Plateau [Master Dissertation]. Jilin University (in Chinese with English abstract).
Zhu, D.C., Pan, G.T., Mo, X.X., Wang, L.Q., Liao, Z.L., Zhao, Z.D., Dong, G.C., Zhou, C.Y., 2006. Late Jurassic-Early Cretaceous geodynamic setting in middle-northern Gangdese: new insights from volcanic rocks. Acta Petrol. Sin. 22 (3), 534–546 (in Chinese with English abstract).
Zhu, D.C., Pan, G.T., Chung, S.L., Liao, Z.L., Wang, L.Q., Li, G.M., 2008. SHRIMP zircon age and geochemical constraints on the origin of Lower Jurassic volcanic rocks from the Yeba Formation, southern Gangdese, South Tibet. Int. Geol. Rev. 50 (5), 442–471.
Zhu, D.C., Mo, X.X., Niu, Y., Zhao, Z.D., Wang, L.Q., Liu, Y.S., Wu, F.Y., 2009. Geochemical investigation of Early Cretaceous igneous rocks along an east–west traverse throughout the central Lhasa Terrane, Tibet. Chem. Geol. 268 (3–4), 298–312.
Zhu, D.C., Mo, X.X., Zhao, Z.D., Niu, Y., Wang, L.Q., Chu, Q.H., Pan, G.T., Xu, J.F., Zhou, C.Y., 2010. Presence of Permian extension- and arc-type magmatism in southern Tibet: paleogeographic implications. Geol. Soc. Am. Bull. 122 (7–8), 979–993.
Zhu, D.C., Zhao, Z.D., Niu, Y., Dilek, Y., Mo, X.X., 2011a. Lhasa terrane in southern Tibet came from Australia. Geology 39 (8), 727–730.
Zhu, D.C., Zhao, Z.D., Niu, Y., et al., 2011b. The Lhasa Terrane: record of a microcontinent and its histories of drift and growth. Earth Planet. Sci. Lett. 301 (1–2), 241–255.
Zhu, D.C., Zhao, Z.D., Niu, Y., Dilek, Y., Hou, Z.Q., Mo, X.X., 2013. The origin and pre-Cenozoic evolution of the Tibetan Plateau. Gondwana Res. 23 (4), 1429–1454.
Zhu, D.C., Li, S.M., Cawood, P.A., Wang, Q., Zhao, Z.D., Liu, S.A., Wang, L.Q., 2016. Assembly of the Lhasa and Qiangtang terranes in central Tibet by divergent double subduction. Lithos 245, 7–17.